

RESEARCH ARTICLE

Variation in limb loading magnitude and timing in tetrapods

Michael C. Granatosky^{1,*}, Eric J. McElroy², Pierre Lemelin³, Stephen M. Reilly⁴, John A. Nyakatura⁵, Emanuel Andrada⁶, Brandon M. Kilbourne⁷, Vivian R. Allen⁸, Michael T. Butcher⁹, Richard W. Blob¹⁰ and Callum F. Ross¹¹


ABSTRACT

Comparative analyses of locomotion in tetrapods reveal two patterns of stride cycle variability. Tachymetabolic tetrapods (birds and mammals) have lower inter-cycle variation in stride duration than bradymetabolic tetrapods (amphibians, lizards, turtles and crocodylians). This pattern has been linked to the fact that birds and mammals share enlarged cerebella, relatively enlarged and heavily myelinated Ia afferents, and γ -motoneurons to their muscle spindles. Both tachymetabolic tetrapod lineages also possess an encapsulated Golgi tendon morphology, thought to provide more spatially precise information on muscle tension. The functional consequence of this derived Golgi tendon morphology has never been tested. We hypothesized that one advantage of precise information on muscle tension would be lower and more predictable limb bone stresses, achieved in tachymetabolic tetrapods by having less variable substrate reaction forces than bradymetabolic tetrapods. To test this hypothesis, we analyzed hindlimb substrate reaction forces during locomotion of 55 tetrapod species in a phylogenetic comparative framework. Variation in species means of limb loading magnitude and timing confirm that, for most of the variables analyzed, variance in hindlimb loading and timing is significantly lower in species with encapsulated versus unencapsulated Golgi tendon organs. These findings suggest that maintaining predictable limb loading provides a selective advantage for birds and mammals by allowing energy savings during locomotion, lower limb bone safety factors and quicker recovery from perturbations. The importance of variation in other biomechanical variables in explaining these patterns, such as posture, effective mechanical advantage and center-of-mass mechanics, remains to be clarified.

KEY WORDS: Locomotion, Sensorimotor, Golgi tendon organs, Predictability, Bradymetabolic, Tachymetabolic

¹Department of Anatomy, New York Institute of Technology, Old Westbury, NY 11568, USA. ²Department of Biology, College of Charleston, Charleston, SC 29424, USA. ³Division of Anatomy, Department of Surgery, University of Alberta, Edmonton, AB, Canada, T6G 2H7. ⁴Department of Biological Sciences, Ohio University, Athens, OH 43210, USA. ⁵Institut für Biologie, Humboldt-Universität zu Berlin, 10115 Berlin, Germany. ⁶Institute of Zoology and Evolutionary Research, Friedrich-Schiller-University Jena, 07749 Jena, Germany. ⁷Museum für Naturkunde, Leibniz Institut für Evolutions- und Biodiversitätsforschung, Invalidenstraße 43, 10115 Berlin, Germany. ⁸Structure and Motion Laboratory, Department of Comparative Biomedical Sciences, The Royal Veterinary College, Hatfield AL9 7TA, UK. ⁹Department of Biological Sciences, Youngstown State University, Youngstown, OH 44555, USA. ¹⁰Department of Biological Sciences, Clemson University, SC 29634, USA. ¹¹Department of Organismal Biology and Anatomy, University of Chicago, Chicago, IL 60637, USA.

*Author for correspondence (michael.granatosky@nyit.edu)

 M.C.G., 0000-0002-6465-5386; V.R.A., 0000-0003-4077-0088

Received 8 February 2019; Accepted 22 November 2019

INTRODUCTION

Comparative analyses of cyclical locomotion and chewing in tetrapods reveal two patterns of variation in cycle duration (Gintof et al., 2010; Ross et al., 2007, 2010, 2013). Tachymetabolic tetrapods, including birds and mammals, have relatively low levels of variation in stride duration between cycles – high rhythmicity – compared with bradymetabolic tetrapod lineages such as amphibians, lizards, turtles and crocodylians (Ross et al., 2007, 2010, 2013). This higher rhythmicity in birds and mammals, which share a high metabolic rate (Nagy, 1987, 2005; Nagy et al., 1999), is argued to be advantageous because it is more energetically efficient, postponing or minimizing fatigue in these highly active animals (O'Connor et al., 2012; Ross et al., 2013). Higher rhythmicity also allows coordination and synchronization of cyclic movements, including tuning of locomotor and ventilation systems (Boggs, 2002; Carrier and Farmer, 2000; Nassar et al., 2001), coordination of jaw and tongue oscillations (Hiemae and Palmer, 2003; Hiemae et al., 1995; Palmer et al., 1997), and minimization of interlimb interference and obstacle avoidance during locomotion (Armstrong and Drew, 1985; Drew et al., 2002, 2004; English, 1989; Serrien et al., 2001).

The neuromuscular basis for high rhythmicity of the cyclic movements of birds and mammals is hypothesized to lie with an enlarged cerebella, relatively enlarged and heavily myelinated Ia afferents, and γ -motoneurons to their muscle spindles (Ross et al., 2013). The cerebellum is an important regulator of predictive and responsive correction of external perturbations (Aoi et al., 2013; Butler and Hodos, 2005; Ross et al., 2013). Selective damage or degeneration of the cerebellum or its afferent and efferent neural pathways results in impaired interlimb coordination (Aoi et al., 2013; English, 1989; Fortier et al., 1987; Ichise et al., 2000; Morton and Bastian, 2006; Yanagihara et al., 1993). Birds and mammals have convergently evolved relatively enlarged lateral cerebella (Butler and Hodos, 2005), along with larger and more complex input and output nuclei (Appelberg et al., 1975; Johansson, 1988; ten Donkelaar, 1988; Wild and Williams, 2000).

Muscle spindle primary afferents – type Ia nerve fibers – convey information from muscle spindles to the central nervous system (CNS) about the rate of change in the length of fibers within a muscle fascicle (Purves and Fitzpatrick, 2001). Afferent information about velocity changes in limb muscles is necessary for coupling limb movements to alternating bursts of motor activity from spinal central pattern generators (Verdaasdonk et al., 2006). Furthermore, stronger afferent proprioceptive signals are associated with less variable cycle frequency (Ausborn et al., 2007). Deafferentation of spinal cord central pattern generators renders them incapable of compensating for variation in external forces and displacements associated with variably disrupted coordination (Allum et al., 1998; Grillner and Zangger, 1979, 1984; Wetzell et al., 1976). Bird and mammal type Ia afferents are myelinated and larger than those of other tetrapods, facilitating rapid conduction of

spindle afferent information to the CNS (Matthews, 1972; Prochazka et al., 2002; Romanovsky et al., 2007). Birds and mammals are also distinctive in having γ -motoneuron innervation of muscle spindle contractile elements, independent of the motor supply to the extrafusal fibers (Bilo et al., 1980; Hulliger, 1984; James and Meek, 1973; Maier, 1992; Ovalle, 1976; Proske, 1997). The γ -motoneurons allow spindle response properties to be tuned independently of extrafusal muscle activity in anticipation of movements and postural adjustments (Proske, 1997; Riemann and Lephart, 2002; Ross et al., 2013; Shneider et al., 2009).

In addition to their more enlarged cerebella, larger and myelinated type Ia afferents, and γ -motoneurons, birds and mammals also have distinctive Golgi tendon organ (GTO) morphology (Fig. 1). The GTO is a specialized mechanoreceptor found in most skeletal muscles (Proske, 1979; Purves and Fitzpatrick, 2001). It lies in series between small groups of muscle fibers and their tendon or aponeurosis of origin or insertion (Huber and Dewitt, 1900; Proske, 1979). Typically, GTOs are distributed unevenly across muscle–tendon junctions, being most densely concentrated in the deep areas of the muscle (Horcholle-Bossavit et al., 1990; Mileusnic and Loeb, 2009). Often considered a protective organ, GTOs are known to be responsive over a wide range of normal physiological muscle forces (Crago et al., 1982; Houk and Henneman, 1967; Mileusnic and Loeb, 2009; Proske, 1979), so it is likely that GTOs have dual sensory roles in the protective Golgi tendon reflex at larger forces and in maintaining consistent limb loading conditions during normal behaviors (Alneas, 1967; Crago et al., 1982; Houk and Henneman, 1967; Mileusnic and Loeb, 2009). GTOs are present in the tendons of fishes, amphibians, reptiles, birds and mammals (Huber and Dewitt, 1900; Proske, 1979). The GTOs of most bradymetabolic tetrapods are free-endings located in tendons some distance from the muscle–tendon junction (Gregory and Proske, 1975; Huber and Dewitt, 1900; Proske, 1979), suggesting that they signal levels of tension across the whole muscle (Proske, 1979). In contrast, in birds and mammals, encapsulated tendon organs are located directly at the muscle–tendon junction (Gregory et al., 2002; Haiden and Awad, 1981; Huber and Dewitt, 1900; Proske, 1979)

where muscle fibers insert into collagen bundles lying within the receptor capsule. This anatomical arrangement enables fine-scale signaling of tension in discrete portions of muscles (Mileusnic and Loeb, 2009), allowing more precise CNS control and predictability of forces generated by the muscles (Alneas, 1967; Crago et al., 1982; Houk and Henneman, 1967; Mileusnic and Loeb, 2009). Interestingly, the GTOs of turtles exhibit features resembling both bradymetabolic and tachymetabolic tetrapods, where some encapsulation of the GTOs is visible near the muscle–tendon junction, but non-encapsulated or free-endings are also present deeper in the tendon (Huber and Dewitt, 1900). Currently, we know little about the GTO morphology of crocodylians and monotremes.

Differences in rhythmicity between tachymetabolic and bradymetabolic tetrapods have been identified in limb step cycle duration (Granatosky et al., 2018a; Ross et al., 2013), but these data do not directly refer to variability in the locomotor forces. One important question is whether substrate reaction forces are also less variable in taxa with low variation in step cycle duration. Maintaining a predictable limb loading environment may have important consequences for overall cost of locomotion (O'Connor et al., 2012; Verdaasdonk et al., 2006), limb bone safety factors (Bertram and Biewener, 1988; Blob et al., 2014; Lowell, 1985) and the ability to recover from unexpected obstacles or perturbations to locomotion (Daley et al., 2006). These factors may be especially important for birds and mammals, which have greater daily travel distances (Daley et al., 2016; Jedrzejewski et al., 2001; Klaassen et al., 2008; Marcus Rowcliffe et al., 2012; Stark et al., 2005; Thompson, 1992; Thompson et al., 1999) and higher metabolic costs than bradymetabolic tetrapods (Nagy, 1987, 2005; Nagy et al., 1999). In this study, we used hindlimb substrate reaction forces collected during locomotion of 55 tetrapod species to test the following hypothesis: tetrapods with encapsulated GTOs have less-variable substrate reaction forces than species with unencapsulated GTOs. Corroboration of this hypothesis would support links between the degree of rhythmicity in cycle duration and predictability in the forces acting on the hindlimbs during locomotion.

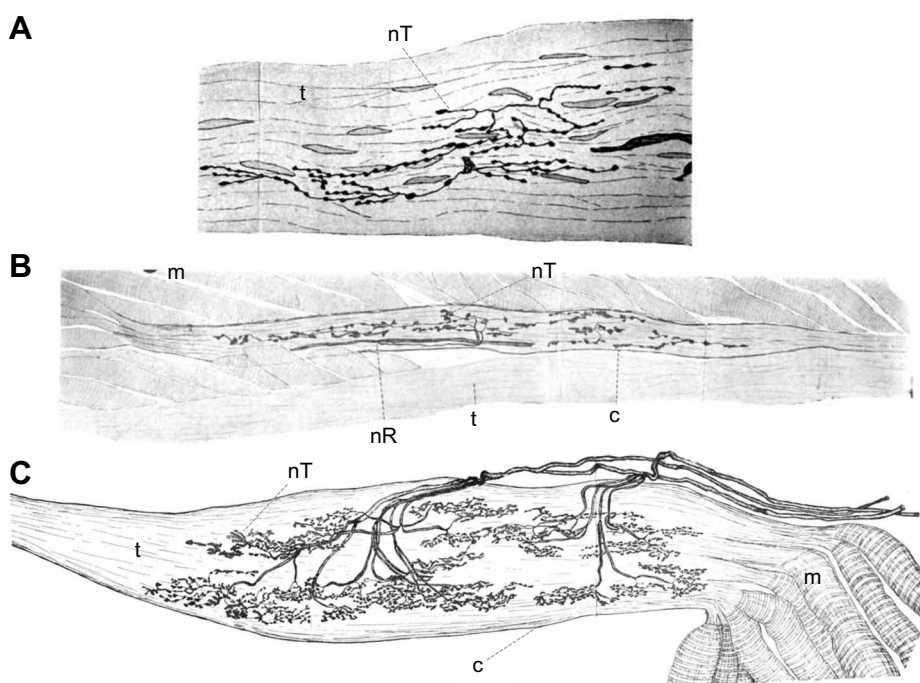


Fig. 1. Histological preparations of the Golgi tendon organs from bradymetabolic and tachymetabolic tetrapods. (A) Amphibian, (B) bird and (C) mammal. Representative histological sections were prepared specifically from m. tibialis posterior of a frog, an undisclosed wing muscle of a dove and an undisclosed hindlimb muscle of a rabbit. nT, terminations of nerve fibers; t, tendon; m, striated muscle fibers; nR, nodes of Ranvier; c, capsule of neuro-tendinous end organs. Figures adapted from Huber and Dewitt (1900) with permission. All information about histological preparation and imaging is available in Huber and Dewitt (1900).

axis, medially oriented substrate reaction force as a negative value on the mediolateral axis, and laterally oriented substrate reaction force as a positive value on the mediolateral axis.

Inter-cycle variation in limb loading was assessed using the coefficient of variation (CV*) of peak forces and of the timing of these peaks within each stance phase. Coefficients of variation were calculated within individuals for each species using $CV^* = (1 + 1/4n)CV$, where n is equal to the number of strides. The CV* of stride cycle duration was also calculated for each individual. The inclusion of n in the calculation of CV* provides an unbiased approximation of relative variance when sample size is low (Sokal and Rohlf, 2012). Because of the limited number of isolated hindlimb substrate reaction forces available for *Pleurodeles waltl* (i.e. one hindlimb substrate reaction force per individual), data for this species were combined for all statistical analyses. The CV* of stride cycle duration for *P. waltl* was calculated from data in Karakasiliotis et al. (2016) and for *Recurvirostra avosetta*, *Haematopus ostralegus* and *Vanellus vanellus* from data in Kilbourne et al. (2016).

For all analyses, variables were \log_{10} -transformed to more closely approximate normality and reduce the potentially confounding effects of extreme values (Keene, 1995; Sokal and Rohlf, 2012). The species-mean CV* of all limb loading variables and stride cycle durations were compared between species with unencapsulated versus encapsulated GTOs using a series of Mann–Whitney U -tests. Despite an attempt to approximate normality in the dataset via \log_{10} transformation, the Mann–Whitney U -test remained the preferred conservative method of analyses because of the small sample sizes (e.g. 55 species) (Sokal and Rohlf, 2012). Mann–Whitney U -tests were conducted in MATLAB (v.2017b; MathWorks). Although information about GTO morphology is lacking for crocodylians, data collected from *Caiman crocodylus* were analyzed along with those for other bradymetabolic tetrapods following Ross et al. (2013).

It is important to note that several variables are thought to affect variation in force magnitude and timing (see Table S1). Consequently, it may be the case that statistical differences observed via Mann–Whitney U -tests described above do not effectively address the potentially influential effects of these confounding variables. As such, we conducted a series of linear mixed-effects models to assess the relationship between the variables of interest with species nested within GTO morphology as a random effect, and GTO morphology (i.e. encapsulated versus unencapsulated), substrate, number of hindlimb substrate reaction forces analyzed, body mass and contact time as fixed effects. As it is well known that speed has a substantial effect on both force magnitude and the shape of force profiles (but see Figs S1 and S2), it is important to consider speed and variation in speed as additional fixed effects. However, because of the large disparity of body sizes analyzed within this study, considering speed and variation in speed without considering potential scaling effects is untenable. As such, dimensionless speed (i.e. speed divided by the square root of acceleration due to gravity multiplied by leg length: s/\sqrt{gL}) and variation in dimensionless speed were utilized instead and included in the model as additional fixed effects. Hindlimb length for each individual was determined from direct measurements from the animals, calibrated space in video recordings, the literature (Karakasiliotis et al., 2016), or based on a closely related taxon (hindlimb length for *Ambystoma mexicanum* was based on data from *A. tigrinum*). Preliminary model runs included the interaction between GTO morphology and mass, dimensionless speed, dimensionless speed CV* and contact time; however, these interactions were only rarely significant (3 out of 44). This indicates that the slope of

relationships between limb loading/timing CV* and mass, dimensionless speed, dimensionless speed CV* and contact time does not differ between GTO morphologies. Thus, none of these interactions were included in the full models. As the goal of this study was to investigate the influence that GTO morphology has on limb loading magnitude and timing, we constrained comparison of our full model to a single null that did not include GTO morphology as a fixed effect, nor did it include the GTO nesting (i.e. species was an un-nested random effect in the null model). The Burnham and Anderson (2001) approach for model comparison was used and Akaike's information criterion (AIC) generated for each model. AIC provides a measure of the goodness of fit of an estimated model and an operational way of trading off the complexity of an estimated model against how well the model fits the data. The best model has the lowest AIC and the significance of full models versus the null models was tested using likelihood ratio tests. Linear mixed-effects models were constructed and analyzed in R using 'lme4' (Bates et al., 2014) following Winter (2013 preprint). Individual CV* for each of the variables of interest were used to construct linear mixed-effects models. Mass, dimensionless speed, dimensionless speed CV*, contact time and number of trials were centered and scaled prior to analysis.

Phylogenetic relatedness between sample taxa may influence these statistical analyses (Felsenstein, 1985; Garland et al., 1992), so we took the following steps to account for these effects in our comparisons. First, we generated a sample of 100 phylogenetic trees to account for phylogenetic uncertainty using the template of a recently published study on European tetrapods (Roquet et al., 2014). To do this, we first built the trunk of the phylogenetic tree to include the most recent common ancestor (mrca) of each of the following crown groups: Amphibia, Mammalia, Lepidosauria, Testudines, Crocodylia and Aves. Tree topology was fixed to widely accepted relationships among these major groups and the depth of each mrca node was fixed to the mean value reported at www.timetree.org (Hedges et al., 2006, 2015; Kumar and Hedges, 2011; Kumar et al., 2017). Next, we grafted samples of trees for each crown group onto this trunk. To do this, we retrieved 1000 posterior samples of trees from www.vertlife.org/phylosubsets that were generated from phylogenetic analyses of squamates (Tonini et al., 2016), birds (Jetz et al., 2014) and amphibians (Jetz and Pyron, 2018). We used a posterior sample of 100 trees for mammals (Kuhn et al., 2011), which are based on a recent supertree analysis (Hedges et al., 2006, 2015; Kumar and Hedges, 2011; Kumar et al., 2017). Our dataset had three turtle species; therefore, we set the branching time between these taxa using values from www.timetree.org (Hedges et al., 2006, 2015; Kumar and Hedges, 2011; Kumar et al., 2017). We then randomly chose one sample of each of these trees, then grafted them onto the appropriate node. We repeated this procedure 100 times to produce a posterior sample of 100 trees that accounted for uncertainty in branch length and topology. These trees were not ultrametric because of the decimal precision of the branch length estimates in the grafted trees; therefore, we forced them to be ultrametric by adding small amounts of branch lengths as needed (see <http://blog.phytools.org/2017/03/forceultrametric-method-for-ultrametric.html> for additional explanation). The final sample of 100 ultrametric, dated phylogenetic trees was used in all subsequent analyses. The maximum clade credibility tree from this sample had 100% nodal support for all nodes except for: (1) the node connecting *Varecia variegata* and *Lemur catta*, which had 60% support and (2) the node connecting *Meleagris gallopavo* and *Gallus gallus*, which had 52% support. The results of subsequent

comparative analyses are presented as the mean±s.d. of the test statistic as computed from the sample of 100 trees. R-packages used to construct the trees included ‘ape’ (Paradis et al., 2004) and ‘phangorn’ (Schliep, 2011).

We tested whether species-mean CV* of limb loading variables and stride cycle duration differed between tetrapods with encapsulated versus unencapsulated Golgi tendon morphology by fitting four different evolutionary models to our data given our sample of phylogenetic trees. The first two models were a single rate Brownian motion model (BM-1) and a single optimum Ornstein–Uhlenbeck model (OU-1) (Hansen, 1997). The BM-1 model assumed that the CV* of all limb loading variables and stride cycle duration evolved under a single evolutionary rate. The OU-1 model assumed that only a single evolutionary trait optimum (i.e. one type of Golgi tendon morphology) was present with a parameter α pulling trait evolution towards that optimum. The other two models we fitted were a two-rate Brownian motion model (BM-M) and a two-optimum Ornstein–Uhlenbeck model (OU-M). To fit the BM-M and OU-M models, we assumed that the ancestral condition for tetrapods was unencapsulated GTOs and that the mammalian and avian lineages independently evolved encapsulated GTOs, and then ‘painted’ the internal branches of the phylogeny accordingly (Figs 2–5). We fitted these models over the sample of 100 trees and then computed the mean and standard deviation of parameter estimates across the 100 model fits. To determine which model (BM-1, BM-M, OU-1 or OU-M) was the ‘best’ fit to the data, we computed the small-sample size AIC for each model and computed Akaike weights from the AIC scores (Burnham and Anderson, 2001). We note that majority support for either the OU-M or BM-M model(s) would indicate that GTO morphology was an important predictor of the evolution of CV* of limb loading variables and/or stride cycle duration.

We ran these evolutionary models using two different inputs. First, we used the function `phyl.resid` in *phytools* (Revell, 2012) to fit a phylogenetic, multiple least squares regression with \log_{10} -transformed species mean values for CV* of limb loading variables and stride cycle duration as the responses (separate regression for each response), and with \log_{10} mass, dimensionless speed and dimensionless speed CV* as predictors, all whilst accounting for phylogeny and assuming a Brownian motion model of trait covariance. This function returned a vector of species residuals, which can be interpreted as mass, dimensionless speed and dimensionless speed CV* ‘corrected’ values. These residuals were then used as input for the first set of evolutionary models listed above. For the second set of evolutionary models, we incorporated sampling error because it can have an important impact on analysis (Ives et al., 2007). To do this, we fitted models to the \log_{10} -transformed species mean values for CV* of limb loading variables and stride cycle duration. We used squared standard errors as our estimate of sampling error. Standard errors were computed per species by first computing the mean CV* per variable within each individual sampled, then computing the per-species standard deviation and dividing that standard deviation by the square root of the number of individuals sampled within that species. Some species had only one sampled individual, and thus their standard error could not be computed using this method. For these species, we assumed a standard error that was the arithmetic mean of all other species standard errors. Unfortunately, neither set of models is ‘ideal’. The first set of models accounts for covariates that may influence force or cycle duration variables, but we are unaware of a method to account for species level ‘error’ in the residuals used as input for the first set of models. The second set of models can account for ‘error’ but does not adjust for covariates. In the context of these caveats, we fitted the evolutionary models using the *mvMORPH* package (Clavel et al., 2015).

We computed type I error rates and statistical power for the OU-M models using a simulation approach (Boettiger et al., 2012; Cooper et al., 2016; Schmitz and Higham, 2018). We did this by simulating 100 datasets under a BM-1 model of evolution and an additional 100 datasets under an OU-M model. Starting values for each model were derived from the fit of the first model from our analyses done over the sample of 100 trees, and performed separately for mass/dimensionless speed/dimensionless speed CV corrected limb loading variables, and for raw variables that accounted for intraspecific sampling error. We then fitted the simulated datasets using BM-1 and OU-M and used the results of these fits to compute: (1) the proportion of BM-1 datasets fitted with OU-M models that had lower AIC than BM-1 datasets fitted with BM-1 models (type I error rate) and (2) the proportion of OU-M datasets fitted with OU-M models that had lower AIC than OU-M datasets fitted with BM-1 models (statistical power). We also computed selection opportunity (η), the discrimination ratio (ϕ) and the signal to noise ratio. These three variables are dimensionless quantities that can provide insight into statistical power when using OU-M models (Cressler et al., 2015). We compared our computed values for η , ϕ and the signal to noise ratio with those from a previous simulation study to help better understand our statistical power, given our relatively low sample size (Cressler et al., 2015).

To test whether variation in single limb loading affects overall system rhythmicity, we conducted a series of regression analyses to assess the relationship between species-mean \log_{10} CV* for each of the limb loading variables and CV* of stride cycle duration. A series of phylogenetic least squares regression (PGLS) analyses was also conducted to account for the effect of phylogeny on these relationships using the R-package *phylolm* (Ho and Ané, 2014). Covariance in the PGLS was modeled using Pagel’s λ and using a single-optimum Ornstein–Uhlenbeck model, so two PGLS models were fitted for each limb loading variable. For the Pagel’s λ model, λ can vary between 0 and 1, with 0 being a branch length transformation resulting in a star phylogeny and a λ of 1 resulting in the original phylogeny. Thus, a model fitted using Pagel’s λ estimates the phylogenetic signal in the regression and transforms branch lengths accordingly. We checked for

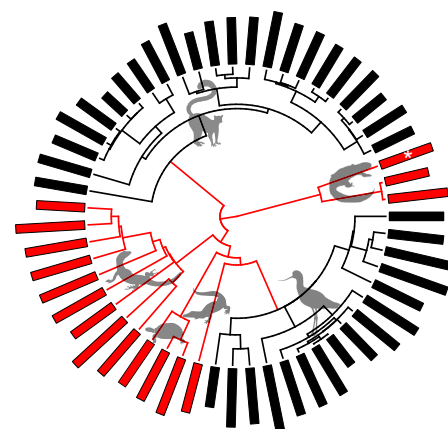


Fig. 3. Phylogeny of species used in this study and bar graphs of \log -transformed mean coefficients of variation (CV*) of stride cycle duration for each species. See Fig. 2 for species names. Coefficients of variation were calculated within individuals for each species using $CV^* = (1 + 1/4n)CV$, where n is the number of strides. Species with encapsulated Golgi tendon organs (GTO) are illustrated in black and species with unencapsulated GTOs are in red. Branch colors on phylogeny correspond to hypothesized ancestral GTO morphology (encapsulated: black, unencapsulated: red). For scale, use *Pleurodeles waltl* (marked with an asterisk) at 1.32.

normality and homoscedasticity of the residuals using diagnostic plots, and no issues were detected. Model fit for each variable was compared using Akaike weights. The P -values of the slope estimates for the best fitting models were corrected for multiple comparisons using the false discovery rate (Benjamini and Hochberg, 1995).

RESULTS

We analyzed 1930 hindlimb substrate reaction forces collected from 150 individuals. As found previously, CV* of stride cycle duration

is lower in animals with encapsulated GTO morphology (Fig. 3). On average, tachymetabolic tetrapods with encapsulated GTO morphology (i.e. mammals and birds) also experience lower variation in peak force magnitude and the timing at which those peak forces occur compared with bradymetabolic tetrapods with unencapsulated GTOs (i.e. amphibians, lizards, turtles and crocodylians) (Tables 1–3, Figs 4 and 5).

Results from Mann–Whitney U -tests revealed significant differences (all $P \leq 0.044$) based on GTO morphology for CV* of

Table 1. Coefficients of variation (CV*) for limb loading magnitude for each of the study species

Species	GTO morphology	Bpk force CV*	Ppk force CV*	Mpk force CV*	Lpk force CV*	Vpk force CV*
<i>Testudo hermanni</i>	Unencapsulated	58.75	35.05	83.00	33.74	9.45
<i>Tiliqua scincoides</i>	Unencapsulated	134.75	57.51	114.88	94.29	33.71
<i>Caiman crocodilus</i>	Unencapsulated	55.57±26.57	43.82±4.52	99.90±9.87	84.34±8.90	17.31±5.43
<i>Smaug warreni</i>	Unencapsulated	940.74±18.99	178.45±145.37	43.86±8.49	27.51±26.16	33.84±6.92
<i>Iguana iguana</i>	Unencapsulated	104.95±6.07	81.04±26.11	99.21±38.17	79.57±3.03	33.46±3.72
<i>Stellagama stellio</i>	Unencapsulated	61.50±46.16	41.79±9.45	57.75±24.88	35.26±22.95	26.68±7.91
<i>Leiocephalus schreibersii</i>	Unencapsulated	184.43±183.35	94.49±27.70	51.00±31.73	46.30±15.02	17.83±5.66
<i>Tropidurus torquatus</i>	Unencapsulated	60.19±16.50	43.18±22.83	40.55±45.86	60.42±48.16	43.01±10.23
<i>Varanus exanthematicus</i>	Unencapsulated	56.84±20.45	28.40±14.67	77.38±45.39	37.48±21.37	23.08±8.73
<i>Oplurus cuvieri</i>	Unencapsulated	47.20±17.48	64.38±16.67	43.07±6.41	37.41±10.57	17.22±11.82
<i>Pleurodeles waltl</i>	Unencapsulated	84.01	31.81	47.75	32.10	12.97
<i>Pseudemys concinna</i>	Unencapsulated	139.27±47.59	168.18±25.78	51.35±7.41	28.93±7.51	10.77±4.15
<i>Salvator merianae</i>	Unencapsulated	184.38±83.09	92.23±33.49	102.16±56.64	53.07±31.07	19.52±7.89
<i>Ambystoma mexicanum</i>	Unencapsulated	1241.07±2041.47	60.34±43.79	64.48±16.87	53.65±9.19	25.55±4.18
<i>Testudo graeca</i>	Unencapsulated	99.37±73.59	74.14±88.58	69.75±7.31	33.82±5.60	4.93±2.51
<i>Ambystoma tigrinum</i>	Unencapsulated	547.55±822.33	91.18±24.26	60.02±18.48	34.34±9.20	32.16±6.89
<i>Ateles fusciceps</i>	Encapsulated	50.02	31.03	84.04	61.64	10.20
<i>Ateles geoffroyi</i>	Encapsulated	48.21	19.61	42.53	49.23	6.79
<i>Erythrocebus patas</i>	Encapsulated	28.09	25.76	113.38	10.64	8.25
<i>Leopardus pardalis</i>	Encapsulated	39.50	16.66	93.11	57.25	20.67
<i>Papio anubis</i>	Encapsulated	22.53	22.48	103.81	15.51	8.38
<i>Alectura lathami</i>	Encapsulated	30.48±9.81	39.81±1.97	38.81±5.64	42.05±0.75	33.77±1.45
<i>Caracara caracal</i>	Encapsulated	37.58±5.53	14.11±10.70	105.34±14.39	29.26±6.56	11.81±7.26
<i>Coturnix coturnix</i>	Encapsulated	30.08±2.72	29.33±3.07	64.93±3.47	50.49±0.05	18.55±1.30
<i>Eudromia elegans</i>	Encapsulated	21.18±8.67	25.65±10.93	44.40±7.15	22.79±5.07	8.45±6.93
<i>Felis catus</i>	Encapsulated	39.75±4.50	20.27±18.20	84.12±19.14	39.92±6.40	6.86±0.02
<i>Hapalemur griseus</i>	Encapsulated	73.51±7.53	47.05±20.91	33.55±5.81	51.31±34.96	19.03±8.29
<i>Leptailurus serval</i>	Encapsulated	21.80±1.76	11.46±7.12	80.81±18.98	31.66±2.91	8.96±4.58
<i>Macaca fascicularis</i>	Encapsulated	72.64±10.59	11.33±2.34	50.67±2.51	116.43±2.32	6.85±3.21
<i>Macaca mulatta</i>	Encapsulated	53.18±22.92	10.95±6.73	11.93±11.52	32.95±8.62	2.04±2.39
<i>Nasua narica</i>	Encapsulated	35.09±7.72	23.55±3.56	140.78±31.49	26.92±8.00	10.36±5.94
<i>Potos flavus</i>	Encapsulated	57.58±1.39	32.60±0.90	52.69±41.56	67.52±3.98	13.97±8.43
<i>Recurvirostra avosetta</i>	Encapsulated	13.56±1.28	17.20±13.94	20.70±2.44	35.26±16.02	7.84±3.44
<i>Struthio camelus</i>	Encapsulated	11.08±0.85	22.17±10.43	25.05±2.82	15.21±16.48	21.28±3.24
<i>Threskiornis molucca</i>	Encapsulated	31.76±13.51	25.68±7.56	73.92±27.05	38.77±24.49	10.95±3.49
<i>Aotus nancymae</i>	Encapsulated	34.27±10.97	35.70±3.75	47.46±9.24	87.23±14.91	9.82±1.72
<i>Cebus capucinus</i>	Encapsulated	45.11±10.81	47.97±17.67	37.12±13.65	51.16±31.24	13.77±7.33
<i>Daubentonia madagascariensis</i>	Encapsulated	69.01±18.32	34.67±10.59	42.52±3.08	72.70±17.61	11.73±2.41
<i>Desmodus rotundus</i>	Encapsulated	53.32±72.66	16.79±15.65	50.73±54.29	66.37±35.30	15.92±15.25
<i>Gallus gallus</i>	Encapsulated	36.91±13.54	45.00±16.00	58.23±22.79	46.15±7.64	15.08±5.72
<i>Lemur catta</i>	Encapsulated	31.56±5.16	25.92±4.50	35.57±6.59	54.78±16.63	11.94±5.41
<i>Numida meleagris</i>	Encapsulated	39.16±8.68	33.07±7.96	51.27±12.78	43.16±14.31	34.26±12.29
<i>Porphyrio porphyrio</i>	Encapsulated	38.44±5.10	36.99±0.83	56.29±20.85	30.01±3.42	17.93±8.60
<i>Propithecus coquereli</i>	Encapsulated	33.67±8.35	17.42±13.40	59.46±10.55	59.68±32.78	13.92±7.48
<i>Varecia variegata</i>	Encapsulated	38.65±14.28	28.47±4.38	29.86±6.69	49.66±12.59	10.47±0.66
<i>Coturnix japonica</i>	Encapsulated	26.24±12.01	30.92±10.89	35.10±23.87	19.89±19.87	14.61±9.19
<i>Haematopus ostralegus</i>	Encapsulated	15.18±5.87	15.46±10.84	33.70±42.51	19.98±15.42	13.29±1.63
<i>Panthera tigris</i>	Encapsulated	18.47±11.12	10.14±5.39	67.57±23.47	41.36±8.26	7.93±2.02
<i>Vanellus vanellus</i>	Encapsulated	19.91±10.64	21.12±15.87	37.60±36.29	29.95±18.52	6.94±4.34
<i>Colinus virginianus</i>	Encapsulated	32.07±12.38	38.92±9.44	28.83±14.06	34.27±14.38	17.14±3.89
<i>Coturnix chinensis</i>	Encapsulated	27.80±4.87	34.18±4.48	44.82±8.68	37.08±10.28	24.19±2.35
<i>Didelphis virginiana</i>	Encapsulated	112.84±114.24	46.93±11.08	66.67±40.42	46.58±6.83	11.87±7.43
<i>Meleagris gallopavo</i>	Encapsulated	37.57±16.00	32.85±9.66	40.06±18.83	32.69±9.31	25.52±6.42
<i>Dromaius novaehollandiae</i>	Encapsulated	18.68±3.26	21.64±3.43	50.23±10.52	36.64±6.31	18.25±3.51
<i>Saimiri sciureus</i>	Encapsulated	63.57±13.42	46.34±7.95	50.82±19.21	82.41±32.02	9.80±1.99

GTO, Golgi tendon organ; Bpk, braking peak; Ppk, propulsive peak; Mpk, medial peak; Lpk, lateral peak; and Vpk, vertical peak. Data are means±s.d.

Table 2. Coefficients of variation (CV*) for the timing of peak force and the braking to propulsive transition for each of the study species

Species	GTO morphology	Timing of Bpk force CV*	Timing of B/P transition CV*	Timing of Ppk force CV*	Timing of Mpk force CV*	Timing of Lpk force CV*	Timing of Vpk force CV*
<i>Testudo hermanni</i>	Unencapsulated	94.74	63.66	35.88	68.48	68.21	40.52
<i>Tiliqua scincoides</i>	Unencapsulated	182.84	149.87	76.13	61.99	98.41	71.27
<i>Caiman crocodilus</i>	Unencapsulated	71.00±5.98	53.38±11.34	21.33±4.69	123.52±3.07	71.45±13.06	37.69±13.47
<i>Smaug warreni</i>	Unencapsulated	59.53	69.72±9.33	18.04±4.30	153.74±57.72	28.42±16.07	24.96±8.87
<i>Iguana iguana</i>	Unencapsulated	85.99±6.15	75.78±27.38	50.80±7.92	154.21±44.40	33.23±19.82	47.40±27.24
<i>Stellagama stellio</i>	Unencapsulated	26.71±24.26	31.81±4.16	18.38±13.89	86.99±55.63	12.02±5.12	21.33±19.24
<i>Leiocephalus schreibersii</i>	Unencapsulated	49.88±28.84	44.60±27.68	37.16±8.21	127.33±39.95	23.00±0.93	18.31±2.47
<i>Tropidurus torquatus</i>	Unencapsulated	82.52±29.45	47.80±10.33	23.74±19.52	26.85±28.48	29.58±10.46	102.35±25.68
<i>Varanus exanthematicus</i>	Unencapsulated	79.00±11.25	48.29±4.85	25.00±9.65	109.93±3.95	25.23±23.46	69.25±51.27
<i>Oplurus cuvieri</i>	Unencapsulated	41.77±5.90	34.99±3.04	22.31±4.93	99.89±11.85	15.30±5.04	17.61±7.11
<i>Pleurodeles waltl</i>	Unencapsulated	162.83	76.71	57.89	80.90	79.79	64.44
<i>Pseudemys concinna</i>	Unencapsulated	94.41±33.77	67.56±26.53	36.37±6.62	71.63±38.31	75.90±37.12	21.16±2.68
<i>Salvator merianae</i>	Unencapsulated	113.59±33.76	77.37±9.08	39.52±2.15	92.89±12.69	70.82±33.65	105.53±28.90
<i>Ambystoma mexicanum</i>	Unencapsulated	131.16±32.84	93.65±65.45	34.96±4.75	106.90±27.03	60.47±27.49	31.22±9.43
<i>Testudo graeca</i>	Unencapsulated	101.72±33.54	44.61±18.79	48.76±16.57	88.01±29.06	38.56±12.46	17.19±2.96
<i>Ambystoma tigrinum</i>	Unencapsulated	107.24±24.05	99.30±26.26	42.63±4.39	126.52±31.45	71.35±15.67	57.74±14.02
<i>Ateles fusciceps</i>	Encapsulated	72.71	50.34	33.18	71.43	79.42	41.07
<i>Ateles geoffroyi</i>	Encapsulated	38.04	13.46	13.20	58.88	41.04	9.86
<i>Erythrocebus patas</i>	Encapsulated	8.35	5.67	2.38	45.42	18.01	9.57
<i>Leopardus pardalis</i>	Encapsulated	22.34	12.21	6.11	103.93	78.02	42.20
<i>Papio anubis</i>	Encapsulated	12.30	12.69	10.94	65.95	64.22	7.39
<i>Alectura lathamii</i>	Encapsulated	19.39±4.08	9.54±3.96	6.69±2.67	76.44±13.98	45.34±1.63	39.43±8.30
<i>Caracal caracal</i>	Encapsulated	29.21±9.66	21.22±3.43	9.56±7.53	112.18±89.70	65.29±17.16	32.52±16.48
<i>Coturnix coturnix</i>	Encapsulated	40.11±8.21	25.12±3.52	15.65±1.92	105.90±9.49	32.19±2.24	42.24±3.72
<i>Eudromia elegans</i>	Encapsulated	30.48±3.87	8.21±1.51	10.01±10.12	26.34±17.11	14.90±2.62	14.23±6.34
<i>Felis catus</i>	Encapsulated	16.73±0.68	15.19±2.51	4.52±1.01	84.85±37.73	58.45±15.69	24.26±2.75
<i>Hapalemur griseus</i>	Encapsulated	60.15±28.33	67.60±6.47	30.27±0.65	19.97±2.97	115.23±19.43	29.07±25.06
<i>Leptailurus serval</i>	Encapsulated	13.48±5.73	7.93±3.23	4.60±2.66	96.95±34.14	81.35±18.95	8.96±4.58
<i>Macaca fascicularis</i>	Encapsulated	32.80±5.00	29.90±1.71	15.42±4.01	32.72±1.50	57.21±4.00	11.49±1.41
<i>Macaca mulatta</i>	Encapsulated	17.25±11.15	24.63±0.19	6.75±6.58	45.17±17.65	60.61±32.87	9.89±4.73
<i>Nasua narica</i>	Encapsulated	19.00±3.60	9.39±1.98	7.87±1.49	123.55±12.90	74.37±10.85	28.25±12.32
<i>Potos flavus</i>	Encapsulated	46.44±0.04	39.86±2.62	20.36±8.17	71.57±24.05	64.36±4.13	28.30±8.09
<i>Recurvirostra avosetta</i>	Encapsulated	37.59±8.08	20.17±2.95	7.94±4.08	107.61±18.01	53.83±8.03	7.84±3.44
<i>Struthio camelus</i>	Encapsulated	24.12±4.89	5.05±4.87	14.61±4.33	25.71±22.90	61.76±81.02	34.03±1.49
<i>Threskiornis molucca</i>	Encapsulated	15.95±8.66	11.71±0.31	8.80±0.42	16.06±7.88	43.70±17.70	16.56±0.49
<i>Aotus nancymae</i>	Encapsulated	61.85±36.33	43.22±18.05	24.54±13.49	41.28±7.83	168.45±52.59	36.84±13.57
<i>Cebus capucinus</i>	Encapsulated	48.30±7.04	48.94±17.81	22.74±11.62	64.15±15.43	113.17±32.00	43.55±10.11
<i>Daubentonia madagascariensis</i>	Encapsulated	64.09±1.85	44.20±10.54	31.89±6.27	51.39±4.78	101.43±39.32	17.01±2.70
<i>Desmodus rotundus</i>	Encapsulated	118.73±38.21	92.52±33.08	28.69±1.89	50.49±40.81	60.95±31.89	60.47±29.22
<i>Gallus gallus</i>	Encapsulated	48.44±22.99	14.31±7.59	10.59±4.02	18.25±7.41	49.07±15.77	57.00±19.62
<i>Lemur catta</i>	Encapsulated	25.86±5.36	17.52±4.57	18.00±12.49	72.21±7.13	93.44±40.89	26.40±5.89
<i>Numida meleagris</i>	Encapsulated	22.44±4.77	12.09±0.90	8.19±2.05	49.99±9.59	46.69±14.19	36.67±7.12
<i>Porphyrio porphyrio</i>	Encapsulated	24.51±2.78	9.87±1.32	8.10±3.07	49.79±38.81	33.40±8.65	30.58±10.92
<i>Propithecus coquereli</i>	Encapsulated	17.06±6.65	86.76±34.01	37.61±12.60	69.02±15.58	128.36±31.95	11.90±4.46
<i>Varecia variegata</i>	Encapsulated	38.18±20.03	22.40±9.05	28.04±10.70	108.72±7.33	87.90±31.34	18.66±5.86
<i>Coturnix japonica</i>	Encapsulated	15.17±4.50	20.72±3.22	21.10±13.27	45.78±29.68	39.68±15.68	28.55±19.59
<i>Haematopus ostralegus</i>	Encapsulated	37.43±16.23	21.98±3.29	14.72±1.78	28.13±29.64	15.60±7.85	21.82±11.38
<i>Panthera tigris</i>	Encapsulated	23.85±5.97	11.39±5.97	6.54±3.40	85.06±61.61	62.64±19.88	40.99±28.64
<i>Vanellus vanellus</i>	Encapsulated	29.06±15.43	26.19±11.33	9.66±5.74	123.45±28.16	65.75±20.03	44.16±18.23
<i>Colinus virginianus</i>	Encapsulated	38.87±19.95	23.10±8.77	19.61±9.80	63.45±21.63	30.49±16.91	25.94±15.06
<i>Coturnix chinensis</i>	Encapsulated	41.89±9.01	16.12±4.83	12.10±5.11	46.75±16.15	38.42±13.54	38.57±14.10
<i>Didelphis virginiana</i>	Encapsulated	67.77±29.13	50.36±17.46	18.20±10.67	88.88±19.03	49.31±19.61	33.09±9.94
<i>Meleagris gallopavo</i>	Encapsulated	42.35±9.19	13.65±1.81	7.12±3.67	26.44±9.12	30.44±14.15	29.58±9.91
<i>Dromaius novaehollandiae</i>	Encapsulated	21.88±6.02	6.49±0.62	4.81±0.76	43.01±8.25	53.28±32.23	29.68±11.68
<i>Saimiri sciureus</i>	Encapsulated	81.24±18.25	51.49±17.99	22.73±4.62	71.55±17.05	101.40±33.37	39.37±9.06

GTO, Golgi tendon organ; Bpk, braking peak; B/P, braking to propulsive transition; Ppk, propulsive peak; Mpk, medial peak; Lpk, lateral peak; and Vpk, vertical peak. Data are means±s.d.

stride cycle duration and all limb loading variables, except Lpk CV* and the timing of Lpk CV*. Linear mixed-effects models did reveal the importance of considering other variables in addition to GTO morphology when exploring the causes of variability in limb loading and timing, such as speed, variation in speed, contact time, number of strides, substrate and body mass (Table S1). However, in all cases, except in regards to the timing of Lpk and timing of Vpk CV*, the

inclusion of information about GTO morphology in the linear mixed-effects models resulted in significantly lower AICs (Table 3). Lower AICs indicate that consideration of GTO morphology results in more parsimonious explanations for variability in limb loading and timing than a model that does not include GTO morphology.

The OU-M models were the best fit for six out of 12 limb loading and cycle duration CV* variables when they were corrected for size,

Table 3. Results from non-phylogenetic Mann–Whitney *U*-tests and comparisons of linear mixed-effects models

Variable	Mann–Whitney <i>U</i> -test (<i>P</i> -value)	Linear mixed-effects model	AIC	χ^2	Comparison of linear mixed-effects models (<i>P</i> -value)
Bpk force CV*	<0.001	Null	138.02	31.86	<0.001
		Model	108.16		
Ppk force CV*	<0.001	Null	40.75	26.77	<0.001
		Model	15.98		
Mpk force CV*	0.044	Null	69.07	9.43	0.002
		Model	61.63		
Lpk force CV*	0.640	Null	22.06	4.53	0.033
		Model	19.53		
Vpk force CV*	0.004	Null	24.24	6.94	0.008
		Model	19.30		
Timing of Bpk force CV*	<0.001	Null	−30.39	16.55	<0.001
		Model	−44.95		
Timing of B/P transition CV*	<0.001	Null	−18.23	25.55	<0.001
		Model	−41.78		
Timing of Ppk force CV*	<0.001	Null	36.01	30.89	<0.001
		Model	7.12		
Timing of Mpk force CV*	<0.001	Null	43.57	5.73	0.017
		Model	39.84		
Timing of Lpk force CV*	0.359	Null	−8.30	3.63	0.057
		Model	−9.93		
Timing of Vpk force CV*	0.004	Null	7.30	0.02	0.890
		Model	9.28		

Mann–Whitney *U*-tests were used to compare species-mean CV* of limb loading variables between tetrapods with encapsulated versus unencapsulated GTO morphology. Linear mixed-effects models were used to assess the relationship between the variables of interest with species and subject as random effects, and GTO morphology (i.e. encapsulated versus unencapsulated), substrate, number of hindlimb substrate reaction forces analyzed, body mass, dimensionless speed, variation in dimensionless speed and contact time as fixed effects. Model (d.f.=11) comparison was constrained to a single null (d.f.=10) that did not include GTO morphology as a fixed effect. GTO, Golgi tendon organ; Bpk, braking peak; Ppk, propulsive peak; Mpk, medial peak; Lpk, lateral peak; Vpk, vertical peak; B/P, braking to propulsive transition; and AIC, Akaike's information criterion.

speed and speed CV* (Table 4). OU-1 models were the best fit for the other six limb loading and cycle duration CV* variables, and in all of these cases OU-M models were the second best fit (Table 4). In the second set of models, which accounted for intraspecific sampling error but did not correct for body mass, speed and speed CV*, the OU-M models were the best fit for the timing of Bpk CV*, timing of Ppk CV*, timing of Lpk CV* and timing of B/P CV*, while BM-M models were the best fit for timing of Vpk CV* and Bpk CV*. OU-1 and BM-1 models were the best fit for the other six variables (Table S2). On average, the OU-M/BM-M models were favored in 50% of the cases, suggesting GTO morphology has evolved towards distinct optima and/or at distinct rates for some limb loading variables but not others. Simulations and computed values of η , ϕ and the signal to noise ratio all suggest moderate to high statistical power for most variables [Table S3; but see Cressler et al. (2015) for a cautious note on interpreting these values], meaning that if an OU-M process generated the observed limb loading CV* patterns, then we were likely to detect that process. However, simulations also found inflated type I error rates (mean 0.17, range 0.06–0.25), suggesting that we too often reject a BM-1 model when it might be the 'correct' evolutionary model. Phylogenetic half-life is reasonable for most of the OU-M and OU-1 models (i.e. in the range of the length of the tree, <352 mya; Table 4), although some models that include standard error have a very large half-life, suggesting that traits will never reach their optima (Table S2).

There was a significant relationship between CV* of stride cycle duration and Ppk force CV* ($y=0.29x+0.81$; $P=0.009$), Vpk force CV* ($y=0.35x+0.84$; $P=0.005$) and the timing of Lpk force CV* ($y=-0.29x+1.74$; $P=0.016$) (Fig. S3). PGLS models using Pagel's λ had the highest Akaike weight for all limb loading variables (Table 5). Pagel's λ was ~ 0.3 – 0.4 , suggesting relatively weak phylogenetic signal in the relationships between CV* of stride cycle duration and all limb loading variables. PGLS found no significant

relationships between CV* of stride cycle duration and limb loading variables after accounting for phylogenetic relatedness of sample taxa (Table 5).

DISCUSSION

In general, variance in peak force magnitude and the timing at which those peak forces occur was found to be lower in tachymetabolic tetrapods with encapsulated GTOs (i.e. mammals and birds) than in bradymetabolic tetrapods with unencapsulated GTOs. This is consistent with the hypothesis that birds and mammals have convergently evolved the ability to perceive precise information on muscle tension and as such can maintain a more predictable limb loading environment. That being stated, it is important to recognize several constraints on our experimental design that may limit the scope of its applicability. First, as with many studies that analyze force profiles, variation in locomotor speed across species, individuals and trials can have substantial effects on the interpretation of results (e.g. Bishop et al., 2018; Demes et al., 1994; Granatosky and Schmitt, 2019; Granatosky et al., 2018b). Despite our use of dimensionless speed as a means to address this issue, it remains the case that one cannot discount speed and variation in speed entirely as an explanatory factor when exploring variability in limb loading and timing (Table S1). However, in almost all cases, the inclusion of information about GTO morphology in the linear mixed-effects models results in a more parsimonious explanation of the observed patterns in limb loading variation and timing across the species sampled. As such, we have observed no evidence suggesting that variation in locomotor speed across species, individuals and trials in some way negates the major conclusions of this study. Though we addressed potentially confounding associations with dimensionless speed and dimensionless speed variation through statistical analyses, a more appropriate means of addressing this issue would have been

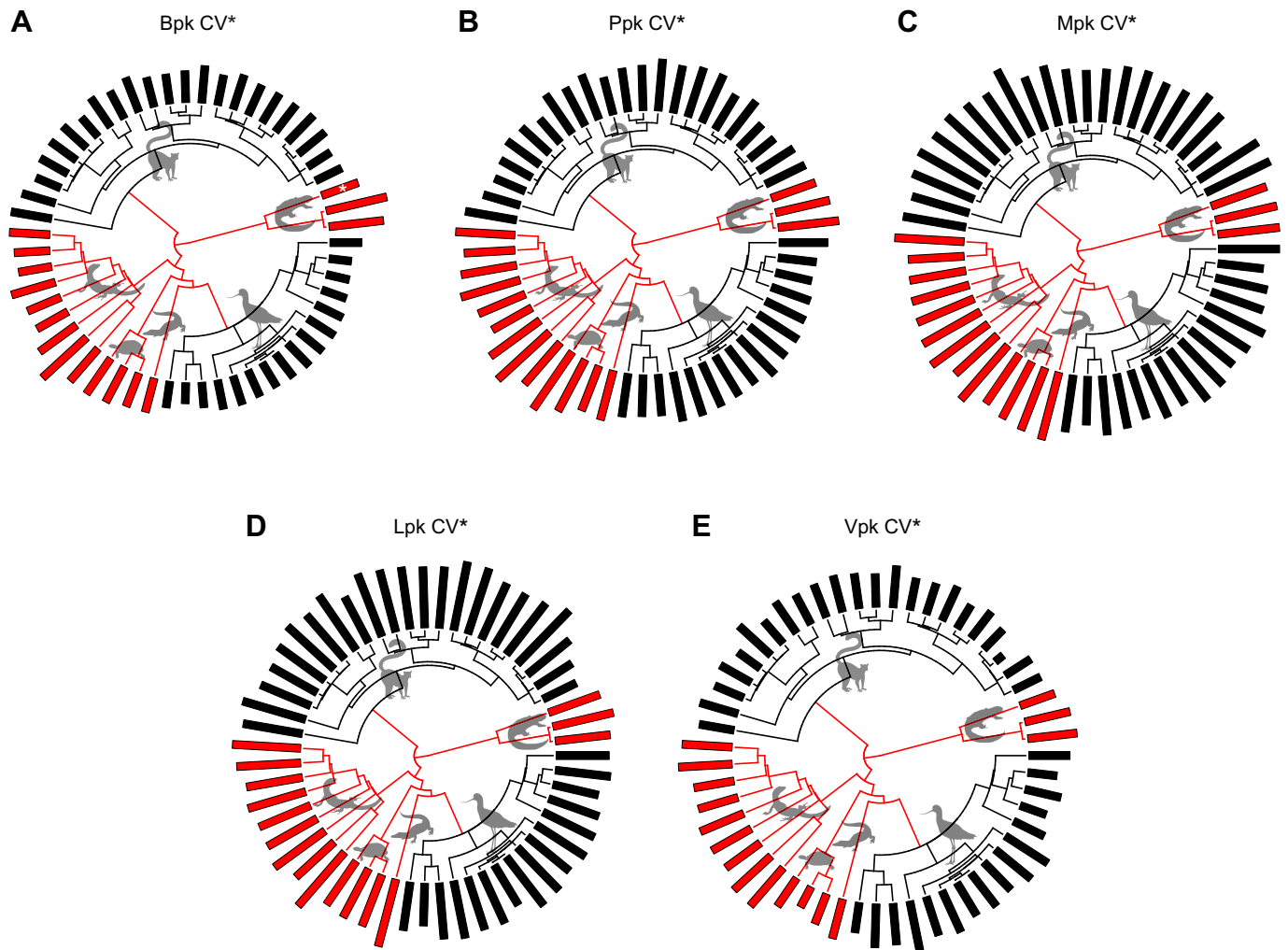


Fig. 4. Phylogeny of species used in this study and bar graphs of log-transformed mean CV* of peak force for each species. (A) Braking peak (Bpk) force, (B) propulsive peak (Ppk) force, (C) medial peak (Mpk) force, (D) lateral peak (Lpk) force and (E) vertical peak (Vpk) force. See Fig. 2 for species names. Coefficients of variation were calculated within individuals for each species using $CV^* = (1 + 1/4n)CV$, where n is the number of strides. Species with encapsulated GTOs are illustrated in black and species with unencapsulated GTOs are in red. Branch colors on phylogeny correspond to hypothesized ancestral GTO morphology (encapsulated: black, unencapsulated: red). For scale, use Bpk CV* for *Pleurodeles waltl* (marked with an asterisk) at 1.92.

more rigorous sampling at the initial experimental stages. Because this study used a combined dataset originating from multiple independent studies of freely moving animals, this was not possible. Future testing of the hypotheses presented here should take all possible precautions to ensure similar speeds, gait types and preferably Froude numbers between individuals, though this may be difficult to achieve across the full diversity of tetrapod species and body designs.

Another potential limitation was based on our goal to use data collected from animals moving on their preferred substrate. No data from arboreal bradymetabolic animals were available, raising the possibility that the observed differences are simply the result of locomotion on different substrates (i.e. arboreal versus terrestrial). Our statistical analyses that account for differences in substrate use suggest no such conclusion, but data on the limb loading behavior of arboreal lizards currently being collected by Knight and Lee (2019) and Munteanu et al. (2019) will help to address this issue. Related to this, postural differences among tetrapods have clear effects on the limb effective mechanical advantage, center-of-mass mechanics, limb kinematics, energetic savings from spring or pendular mechanisms, gait and ecological use of locomotor behaviors

(reviewed by Reilly et al., 2007). Any or all of these factors may explain differences among these taxa in the variation observed in substrate reaction forces, and their covariation makes disentangling their individual effects challenging. That being said, the sprawling locomotion of the common vampire bat (*Desmodus rotundus*) does not appear to influence inter-cycle loading variability compared with the other mammals sampled. Similarly, the ‘intermediate’ postures used by *C. crocodilus* (Nyakatura et al., 2019) appear to do little to differentiate limb loading variation and timing of this taxa from other bradymetabolic tetrapods. Even though these are only two species, these data suggest that posture is less important in driving patterns in force variability than factors related to GTO morphology.

Finally, we acknowledge that our data underrepresent total tetrapod diversity and are skewed towards primates (14/55 species sampled) and tachymetabolic species broadly (39/55 species sampled). Data on forces and GTO anatomy are needed from a greater diversity of species, especially basal mammals, crocodylians and salamanders. Moreover, sampling more species may help to reduce the inflated type I error rates we found associated with the OU-M models (Cooper

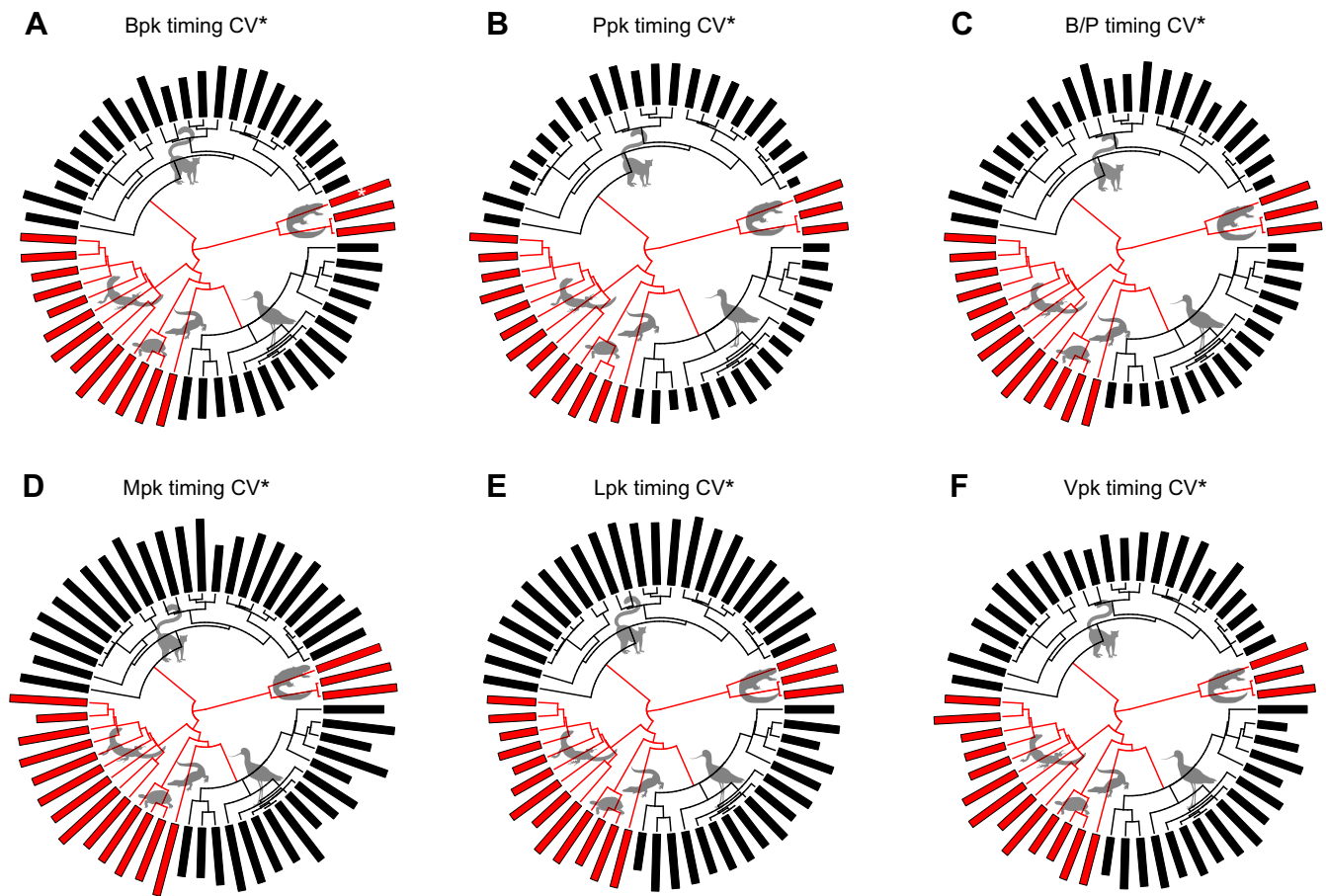


Fig. 5. Phylogeny of species used in this study and bar graphs of log-transformed mean CV* of the timing of peak force for each species. (A) Braking peak (Bpk) force, (B) braking to propulsive transition (B/P), (C) propulsive peak (Ppk) force, (D) medial peak (Mpk) force, (E) lateral peak (Lpk) force and (F) vertical peak (Vpk) force for each species. See Fig. 2 for species names. Coefficients of variation were calculated within individuals for each species using $CV^* = (1 + 1/4n)CV$, where n is the number of strides. Species with encapsulated GTOs are illustrated in black and species with unencapsulated GTOs are in red. Branch colors on phylogeny correspond to hypothesized ancestral GTO morphology (encapsulated: black, unencapsulated: red). For scale, use timing of Bpk CV* for *Pleurodeles waltl* (marked with an asterisk) at 2.21.

et al., 2016). Sampling GTO morphology and forces within a greater diversity of turtles would serve as a powerful test of the link between GTO morphology and force CV* because it would control for metabolic type (i.e. all turtles are bradymetabolic) and it would limit the myriad of confounding variables inherent in sampling at a broad phylogenetic scope, such as all of Tetrapoda.

These concerns notwithstanding and as stated above, analyses of species-mean variation in limb loading magnitude and timing confirm that, for most of the variables analyzed, variance in hindlimb loading is significantly lower in animals with encapsulated versus unencapsulated GTOs. This difference is significant regardless of speed, variation in speed, contact time, number of individuals, number of strides, substrate and body mass. This result has mixed support from the evolutionary analyses; the OU-M models that assume distinct evolutionary trait optima for animals with encapsulated versus unencapsulated GTOs are the best fit for ~50% of the limb loading variables. The large magnitude of the differences in variance between animals with encapsulated versus unencapsulated GTOs in both peak hindlimb forces and the timing of those forces, as well as the persistence of these differences across multiple lineages of birds and mammals, suggest that these clade-specific differences in limb loading provide insight into the functional significance of differences in rhythmicity. Specifically, maintaining a predictable limb loading environment may have important consequences for overall costs of

locomotion (O'Connor et al., 2012; Verdaasdonk et al., 2006), bone safety factors (Bertram and Biewener, 1988; Blob et al., 2014; Lowell, 1985) and the ability to recover from unexpected falls (Daley et al., 2006). We address each of these in turn below.

While the substrate reaction forces examined in this study do not provide a direct measure of force generation by the muscles, the external forces acting on the body during locomotion must be resisted by muscular activity (Beck, 2009; Gray, 1944, 1968). As such, variation in hindlimb substrate reaction forces provides insight into variation in muscle force production during locomotion. The energetic costs of moving the body constitute a high proportion of the overall metabolic budget of an animal (Kram and Taylor, 1990; Pontzer, 2016; Reilly et al., 2007) and the predominant energy-consuming process in locomotion is muscle force production (Kram and Taylor, 1990; Pontzer, 2016). During locomotion on level substrates, muscle forces produced by limb muscles must support body weight and propel the animal forward. To optimize energy expenditure, animals should only apply the amount of force necessary to achieve support, balance and propulsion (O'Connor et al., 2012; Taylor et al., 1980, 1982) as increased variability in muscle force magnitude wastes considerable amounts of energy (Agiouvlatis et al., 2015; Granatosky et al., 2018a; O'Connor et al., 2012; Verdaasdonk et al., 2006). Hence, minimizing variability in muscle force generation contributes to energetic efficiency during steady-state locomotion.

Table 4. Evolutionary models fitted to residual limb loading and stride cycle CV*

Variable	Model	σ^2	α	$T_{1/2}$	θ	AICc	Akaike weights
Bpk force CV*	BM-1	1.0e-3±7.3e-5			0.00±0.00	13.6±2.5	0.15±0.06
	BM-M	1.5e-3±1.3e-4, 0.8e-3±5.7e-5			-0.01±0.00	13.5±2.4	0.15±0.07
	OU-1	1.3e-3±1.6e-4	3.1e-3±9.2e-4	224	-0.05±0.01	13.2±1.5	0.15±0.01
	OU-M	1.5e-3±2.3e-4	5.9e-3±1.7e-3	117	0.10±0.01, -0.88±0.17	10.7±1.3	0.55±0.12
Ppk force CV*	BM-1	6.3e-4±2.2e-5			0.00±0.00	-12.6±1.0	0.00±0.00
	BM-M	5.9e-4±4.5e-5, 6.5e-4±1.6e-5			0.00±0.00	-10.4±1.0	0.00±0.00
	OU-1	9.5e-4±2.6e-5	6.7e-3±1.4e-4	103	0.00±0.01	-18.6±0.9	0.02±0.01
	OU-M	1.6e-3±8.1e-5	2.1e-2±1.3e-3	33	0.14±0.00, -0.23±0.02	-27.3±1.0	0.98±0.01
Mpk force CV*	BM-1	1.8e-3±3.2e-4			0.00±0.00	44.3±7.6	0.00±0.00
	BM-M	8.7e-4±5.8e-4, 2.2e-3±2.2e-4			-0.01±0.00	40.0±10.8	0.00±0.00
	OU-1	8.3e-3±1.1e-3	6.5e-2±2.0e-2	11	0.13±0.04	10.2±11.8	0.68±0.01
	OU-M	9.0e-3±1.3e-3	7.1e-2±1.9e-2	10	0.08±0.01, 0.16±0.07	11.8±12.9	0.32±0.01
Lpk force CV*	BM-1	3.0e-3±8.7e-4			0.00±0.00	72.1±12.6	0.00±0.00
	BM-M	2.0e-3±1.5e-3, 3.5e-3±6.2e-4			-0.01±0.00	70.1±14.5	0.00±0.00
	OU-1	1.6e-2±3.2e-3	8.0e-2±3.0e-2	9	0.23±0.01	34.5±19.4	0.02±0.02
	OU-M	2.6e-2±6.3e-3	1.6e-1±6.2e-2	4	0.02±0.02, 0.34±0.10	26.7±18.4	0.98±0.03
Vpk force CV*	BM-1	1.1e-3±7.7e-5			0.00±0.00	20.0±2.1	0.00±0.00
	BM-M	2.8e-4±4.1e-5, 1.5e-3±1.0e-4			0.01±0.00	8.6±2.7	0.00±0.00
	OU-1	2.4e-3±1.6e-4	1.8-2±1.0e-3	39	0.02±0.02	-1.0±2.7	0.53±0.08
	OU-M	2.5e-3±1.7e-4	2.0e-2±1.7e-3	35	0.10±0.01, -0.04±0.03	-0.7±3.3	0.47±0.09
Timing of Bpk force CV*	BM-1	3.0e-3±9.1e-4			0.00±0.00	71.5±13.4	0.00±0.00
	BM-M	1.7e-3±1.4e-3, 3.6e-3±7.4e-4			0.00±0.00	68.2±16.3	0.00±0.00
	OU-1	5.5e-2±1.7e-2	4.7-1±1.8e-1	1.5	0.02±0.01	8.5±16.3	0.52±0.00
	OU-M	6.0e-2±1.5e-2	5.5e-1±2.0e-1	1.3	0.05±0.01, 0.00±0.11	8.4±17.0	0.48±0.00
Timing of B/P transition CV*	BM-1	1.3e-3±3.3e-5			0.00±0.00	29.0±1.7	0.00±0.00
	BM-M	2.8e-4±1.8e-5, 1.8e-3±4.7e-5			0.01±0.00	16.2±2.0	0.01±0.01
	OU-1	2.7e-3±2.3e-4	1.7e-2±2.0e-3	41	-0.05±0.01	9.8±1.6	0.13±0.03
	OU-M	4.4e-3±3.7e-4	3.5e-2±3.4e-3	20	0.07±0.00, -0.16±0.01	6.0±1.3	0.86±0.04
Timing of Ppk force CV*	BM-1	1.5e-3±1.6e-4			0.00±0.00	33.7±4.3	0.00±0.00
	BM-M	5.7e-4±2.9e-4, 1.9e-3±1.2e-4			0.02±0.00	27.5±7.4	0.00±0.00
	OU-1	2.7e-3±2.2e-4	1.4e-2±1.2e-3	50	-0.08±0.02	16.0±5.7	0.01±0.01
	OU-M	3.7e-3±3.7e-4	2.8e-2±1.4e-3	25	0.09±0.01, -0.27±0.05	7.4±5.7	0.99±0.01
Timing of Mpk force CV*	BM-1	2.2e-3±5.8e-4			0.00±0.00	54.7±11.7	0.00±0.00
	BM-M	1.4e-3±9.2e-4, 2.6e-3±4.6e-4			0.00±0.00	53.6±13.2	0.01±0.00
	OU-1	1.0e-2±1.6e-3	5.7e-2±1.7e-2	12	0.13±0.06	27.0±16.0	0.69±0.09
	OU-M	1.1e-2±2.2e-3	6.2e-2±1.5e-2	11	0.10±0.01, 0.16±0.10	28.7±15.4	0.31±0.09
Timing of Lpk force CV*	BM-1	9.2e-4±8.5e-5			0.00±0.00	8.2±3.4	0.00±0.00
	BM-M	4.2e-4±1.3e-4, 1.1e-3±7.4e-5			0.00±0.00	4.6±5.0	0.01±0.00
	OU-1	1.7e-3±1.4e-4	1.2e-2±3.7e-4	58	-0.06±0.02	-5.8±4.1	0.65±0.07
	OU-M	1.8e-3±1.1e-4	1.4e-2±1.4e-3	50	-0.11±0.00, 0.01±0.04	-4.5±4.6	0.34±0.07
Timing of Vpk force CV*	BM-1	1.7e-3±9.4e-5			0.00±0.00	41.0±1.6	0.00±0.00
	BM-M	6.4e-4±6.6e-5, 2.1e-3±1.2e-4			-0.01±0.00	36.0±1.9	0.00±0.00
	OU-1	4.1e-3±1.7e-4	2.3e-2±1.9e-3	30	0.07±0.02	20.0±3.0	0.76±0.01
	OU-M	4.1e-3±1.7e-4	2.3e-2±1.8e-3	30	0.07±0.01, 0.08±0.03	22.0±2.9	0.24±0.01
Stride cycle duration CV*	BM-1	3.9e-3±1.4e-3			0.00±0.00	85.8±15.6	0.00±0.00
	BM-M	3.3e-3±2.5e-3, 4.3e-3±9.0e-4			0.01±0.01	86.3±16.5	0.00±0.00
	OU-1	2.2e-1±3.6e-1	1.6e0±2.6e0	0.43	-0.24±0.01	37.1±27.4	0.00±0.00
	OU-M	1.4e0±1.3e0	1.0e1±6.6e0	0.06	0.05±0.02, -0.38±0.14	17.1±28.7	1.00±0.00

Residuals are from regressions of \log_{10} limb loading and stride cycle duration CV* on \log_{10} mass, \log_{10} speed and \log_{10} speed CV*. Bold indicates models with the most support. Values presented are means±s.d. based on running the analysis on 100 trees to account for phylogenetic uncertainty. Variables are defined as follows: σ^2 , Brownian motion rate parameter; α , strength of pull towards trait optimum under OU model; $T_{1/2}$, phylogenetic half-life; θ , trait optima. Models as are defined as follows: BM1, single rate Brownian motion; BM-M, two-rate Brownian motion; OU-1, single optimum Ornstein–Uhlenbeck; OU-M, two optima Ornstein–Uhlenbeck. Bpk, braking peak; Ppk, propulsive peak; Mpk, medial peak; Lpk, lateral peak; Vpk, vertical peak; B/P, braking to propulsive transition; BM-1, single rate Brownian motion model; BM-M, two-rate Brownian motion model; OU-1, single optimum Ornstein–Uhlenbeck model; OU-M, two-optimum Ornstein–Uhlenbeck model; and AICc, small sample size corrected Akaike's information criterion.

Minimizing variation in substrate reaction forces also reduces the likelihood that oscillations of the center of mass and limbs will produce unstable dynamic states (Full et al., 2002; Jordan et al., 2007; O'Connor et al., 2012). In such states, avoiding falling and interlimb interference likely necessitates more muscle recruitment and more work by the limbs and their muscles. For birds and mammals, which have greater daily travel distances (Daley et al., 2016; Jedrzejewski et al., 2001; Klaassen et al., 2008; Marcus Rowcliffe et al., 2012; Stark et al., 2005; Thompson, 1992; Thompson et al., 1999) and higher metabolic costs than bradymetabolic tetrapods (Nagy, 1987,

2005; Nagy et al., 1999), minimizing unnecessary energetic expenditure by maintaining a predictable limb loading environment is likely to have had an important selective benefit.

During locomotion over land, limb bones are exposed to loads and, like most biological structures, they can withstand greater loads than they usually experience, as estimated by their safety factor (Alexander, 1981, 1988; Blob et al., 2014; Lowell, 1985). Among tetrapods, birds and eutherian mammals (opossums have safety factors consistent with bradymetabolic tetrapods; Butcher et al., 2011; Gosnell et al., 2011) have lower limb-bone safety factors than

Table 5. Phylogenetic generalized least squares (PGLS) models of the relationships between coefficient of variation (CV*) of stride cycle duration (y) and CV* of all limb loading variables (x)

Variable	Model	σ^2	α	λ	AIC	Akaike weights	Intercept	Slope	t-value	P-value
Bpk force CV*	λ	0.00013		0.34	-12.7	1.00	1.243	0.018	0.21	0.835
	OU-1	0.10381	1.000		-1.1	0.00	1.151	0.053	0.05	0.497
Ppk force CV*	λ	0.00012		0.28	-13.9	0.98	1.057	0.136	1.15	0.255
	OU-1	0.09238	1.000		-5.3	0.02	0.806	0.288	2.66	0.010
Mpk force CV*	λ	0.00012		0.32	-15.0	1.00	1.634	-0.203	-1.51	0.137
	OU-1	0.09840	1.00		-1.8	0.00	1.719	0.274	-1.82	0.077
Lpk force CV*	λ	0.00013		0.36	-13.8	1.00	1.502	-0.138	-1.04	0.305
	OU-1	0.09970	1.00		-1.1	0.00	1.626	-0.237	-1.59	0.126
Vpk force CV*	λ	0.00013		0.31	-15.1	0.98	1.042	0.196	1.56	0.126
	OU-1	0.08996	1.00		-6.8	0.02	0.846	0.347	2.96	0.006
Timing of Bpk force CV*	λ	0.00013		0.31	-13.5	1.00	1.113	0.094	0.93	0.355
	OU-1	0.10005	1.00		-0.9	0.00	0.995	0.153	1.55	0.127
Timing of B/P transition CV*	λ	0.00013		0.32	-13.5	1.00	1.153	0.078	0.893	0.376
	OU-1	0.10267	1.00		0.5	0.00	1.116	0.088	1.032	0.308
Timing of Ppk force CV*	λ	0.00013		0.32	-13.3	1.00	1.178	0.074	0.76	0.448
	OU-1	0.10080	1.00		-0.5	0.00	1.077	0.136	1.43	0.158
Timing of Mpk force CV*	λ	0.00014		0.35	-12.8	1.00	1.358	-0.042	-0.36	0.722
	OU-1	0.10416	1.00		1.3	0.00	1.347	-0.057	-0.44	0.672
Timing of Lpk force CV*	λ	0.00013		0.32	-12.8	0.98	1.357	-0.046	-0.37	0.713
	OU-1	0.09427	1.00		-4.2	0.02	1.738	-0.289	-2.43	0.020
Timing of Vpk force CV*	λ	0.00013		0.34	-13.4	1.00	1.151	0.083	0.803	0.426
	OU-1	0.09998	1.00		-0.9	0.00	0.983	0.180	1.586	0.124

Bold indicates models with the most support. Values presented are means based on running the analysis on 100 trees to account for phylogenetic uncertainty (standard deviations not shown, but were at least an order of magnitude smaller than the mean for all parameters). Variables defined as follows: σ^2 , Brownian motion rate parameter; α , strength of pull towards trait optimum under OU-1 model; λ , Pagel's lambda. Models defined as follows: λ , Pagel's lambda model; OU-1, single optimum Ornstein–Uhlenbeck. Bpk, braking peak; Ppk, propulsive peak; Mpk, medial peak; Lpk, lateral peak; Vpk, vertical peak; B/P, braking to propulsive transition; and AIC, Akaike's information criterion.

do other tetrapod lineages (Blob et al., 2014), possibly as a result of the greater predictability of the loads (Bertram and Biewener, 1988; Blob et al., 2014; Lowell, 1985). We hypothesize that improved predictability of dynamic loading facilitates the capacity of birds and mammals to operate successfully with lower limb bone safety factors, making it possible to reduce energetic costs as well (Alexander, 1997; Lowell, 1985).

The data presented here suggest that the limbs of birds and mammals experience reduced variability in external forces compared with other tetrapod lineages. We speculate that this is in part due to anticipatory modulation of reflexes through γ -motoneurons and enlarged cerebella, as well as to enhanced precision of their GTO system compared with other tetrapods (Gregory and Proske, 1975; Gregory et al., 2002; Haiden and Awad, 1981; Huber and Dewitt, 1900; Proske, 1979). At present, we know little about the control strategies that tetrapods use to maintain stability in the face of the unexpected obstacles they experience in their natural environment. Daley and colleagues (2006) addressed this question by perturbing the running of guinea fowl with an unexpected drop in substrate height. To avoid instability upon encountering a sudden drop, the bird must dissipate energy, convert it to another form, or perform both in combination (Biewener and Daley, 2007; Daley et al., 2006). Interestingly, guinea fowl adopt a range of these strategies across a continuum that relates to magnitude and direction of the substrate reaction force. When animals experience an unexpected perturbation, limb muscles must activate with the appropriate timing and intensity to resist substrate reaction forces and provide the appropriate leg stiffness (Daley et al., 2006). The activation level of the limb muscles depends on a combination of feed-forward, rhythmic motor control and proprioceptive feedback, including muscle stretch (spindle organs) and GTOs (Grillner, 1975; Pearson et al., 1998). The derived GTO morphology of birds and mammals and the increased predictability of rhythmic movements may allow birds and mammals

to return to a state of dynamic stability after an unexpected fall quicker than animals with unencapsulated GTOs. Future work in this area is required to test this hypothesis.

While variation in limb loading does appear to be largely driven by differences in GTO morphology, the magnitude of this variation is largely variable dependent. Namely, propulsive and braking forces show the greatest disparity between species with encapsulated versus unencapsulated GTOs. This is followed by vertical forces, and much smaller differences are observed in mediolateral forces, which tend to be highly variable across strides for all species. Arguably, there are functional reasons and consequences associated with these findings. As articulated by Bishop et al. (2018), mediolateral forces are probably only (or at least predominantly) exerted for stabilization purposes. That is, they reflect small-scale, step-to-step adjustments made by the animal in order to maintain dynamic stability. Therefore, rather than being an important motor goal to achieve straight-line locomotion, mediolateral forces may be viewed as a constraint: simply apply whatever mediolateral force is necessary at each instant in time to maintain dynamic stability. Furthermore, because mediolateral forces tend to be relatively small compared with vertical and fore–aft force components, even in sprawling taxa, small fluctuations about the mean result in substantially greater variance (Sokal and Rohlf, 2012). Vertical forces are usually the largest that an animal exerts and primarily serve to support the body against gravity (Gray, 1944). As such, maintaining appropriate vertical forces is essential to preventing an animal from collapsing. As a result, there is likely less room for variance in this loading parameter compared with the other force components. In terms of both timing and magnitude, variation in propulsive and braking forces is greatest between sample taxa. These fore–aft forces functionally serve to keep the animal moving forward and inhibit out-of-control momentum of the center of mass (Granatosky et al., 2018b; Gray, 1944). Thus, propulsive and braking forces likely most influence overall system

rhythmicity, which, as discussed above, has clear selective advantages for birds and mammals. It is also the case that fore–aft forces most strongly correlate with overall external morphology of bony structures (Fabre et al., 2016). This relationship may explain the overlapping patterns in bone safety factors observed by Blob et al. (2014) and the findings of this study.

Conclusions

This study demonstrates that, in addition to having less-variable cycle durations, tachymetabolic tetrapods (i.e. birds and mammals) also exhibit lower variation in limb loading magnitude and timing during locomotion compared with bradymetabolic tetrapods (i.e. amphibians and reptiles). The ability of birds and mammals to monitor and correct force variability could be linked to neural specializations such as encapsulated GTOs positioned near the muscle–tendon junction, along with the presence of γ -motoneurons and enlarged afferents and cerebella. We hypothesize that a predictable limb loading environment is advantageous for birds and mammals by allowing energy savings during locomotion, lower safety factors in limb bones and quicker recovery from perturbations.

Acknowledgements

We thank all those who helped with animal care and use. Without their help, we would not have been able to complete this study. We thank Daniel Schmitt, J. D. Laurence-Chasen, Mark Westneat and two anonymous reviewers for their comments, which improved the overall quality of this work.

Competing interests

The authors declare no competing or financial interests.

Author contributions

Conceptualization: M.C.G., C.F.R.; Methodology: M.C.G., E.J.M., C.F.R.; Validation: C.F.R.; Formal analysis: M.C.G., E.J.M., C.F.R.; Investigation: M.C.G.; Resources: J.A.N.; Data curation: M.C.G., E.J.M., P.L., S.M.R., J.A.N., E.A., B.M.K., V.R.A., M.T.B., R.W.B.; Writing - original draft: M.C.G., C.F.R.; Writing - review & editing: M.C.G., E.J.M., P.L., S.M.R., J.A.N., E.A., B.M.K., M.T.B., R.W.B., C.F.R.; Supervision: M.C.G., C.F.R.; Funding acquisition: M.C.G.

Funding

This study was funded in part by the Leakey Foundation, Force and Motion Foundation, the National Science Foundation's Graduate Research Fellowship Program, and grants BCS 9706676, 0109130, 0240865, 0504685, 0725126, 0725147, 0962682.

Data availability

Additional data, phylogeny and R-scripts used for analyses are available from the figshare repository: <https://figshare.com/s/e3095a4b07376797e92a>

Supplementary information

Supplementary information available online at <http://jeb.biologists.org/lookup/doi/10.1242/jeb.201525.supplemental>

References

- Agiovlasitis, S., McCubbin, J. A., Yun, J., Widrick, J. J. and Pavol, M. J.** (2015). Gait characteristics of adults with Down syndrome explain their greater metabolic rate during walking. *Gait Posture* **41**, 180–184. doi:10.1016/j.gaitpost.2014.10.004
- Alexander, R. M.** (1981). Factors of safety in the structure of animals. *Sci. Prog.* **67**, 109–130.
- Alexander, R.** (1988). Symmorphosis and safety factors. In *Principles of Animal Design* (ed. D. Weibel, C. Taylor and L. Bolis), pp. 28–35. Cambridge: Cambridge University Press.
- Alexander, R. M. N.** (1997). A theory of mixed chains applied to safety factors in biological systems. *J. Theor. Biol.* **184**, 247–252. doi:10.1006/jtbi.1996.0270
- Allum, J. H. J., Bloem, B. R., Carpenter, M. G., Hulliger, M. and Hadders-Algra, M.** (1998). Proprioceptive control of posture: a review of new concepts. *Gait Posture* **8**, 214–242. doi:10.1016/S0966-6362(98)00027-7
- Alneus, E.** (1967). Static and dynamic properties of Golgi tendon organs in the anterior tibial and soleus muscles of the cat. *Acta Physiol. Scand.* **70**, 176–187. doi:10.1111/j.1748-1716.1967.tb03613.x
- Andrada, E., Rode, C., Sutedja, Y., Nyakatura, J. A. and Blickhan, R.** (2014a). Trunk orientation causes asymmetries in leg function in small bird terrestrial locomotion. *Proc. Biol. Sci.* **281**. doi:10.1098/rspb.2014.1405
- Andrada, E., Rode, C., Sutedja, Y., Nyakatura, J. A. and Blickhan, R.** (2014b). Data from: Trunk orientation causes asymmetries in leg function in small bird terrestrial locomotion. *Dryad Digital Repository*. <https://datadryad.org/stash/dataset/doi:10.5061/dryad.jh5h4>
- Andrada, E., Haase, D., Sutedja, Y., Nyakatura, J. A., Kilbourne, B. M., Denzler, J., Fischer, M. S. and Blickhan, R.** (2015). Mixed gaits in small avian terrestrial locomotion. *Sci. Rep.* **5**, 13636. doi:10.1038/srep13636
- Aoi, S., Katayama, D., Fujiki, S., Tomita, N., Funato, T., Yamashita, T., Senda, K. and Tsuchiya, K.** (2013). A stability-based mechanism for hysteresis in the walk–trot transition in quadruped locomotion. *J. R. Soc. Interface* **10**, 20120908. doi:10.1098/rsif.2012.0908
- Appelberg, B., Jeneskog, T. and Johansson, H.** (1975). Rubrospinal control of static and dynamic fusimotor neurones. *Acta Physiol. Scand.* **95**, 431–440. doi:10.1111/j.1748-1716.1975.tb10071.x
- Armstrong, D. M. and Drew, T.** (1985). Forelimb electromyographic responses to motor cortex stimulation during locomotion in the cat. *J. Physiol.* **367**, 327–351. doi:10.1113/jphysiol.1985.sp015827
- Ausborn, J., Stein, W. and Wolf, H.** (2007). Frequency control of motor patterning by negative sensory feedback. *J. Neurosci.* **27**, 9319–9328. doi:10.1523/JNEUROSCI.0907-07.2007
- Bates, D., Mächler, M., Bolker, B. and Walker, S.** (2014). Fitting linear mixed-effects models using lme4. *J. Stat. Soft.* **67**. doi:10.18637/jss.v067.i01
- Beck, B. R.** (2009). Muscle forces or gravity—what predominates mechanical loading on bone? Introduction. *Med. Sci. Sports Exerc.* **41**, 2033–2036. doi:10.1249/MSS.0b013e3181a8c4b6
- Benjamini, Y. and Hochberg, Y.** (1995). Controlling the false discovery rate: a practical and powerful approach to multiple testing. *J. R. Stat. Soc. Ser. B Methodol.* **57**, 289–300. doi:10.1111/j.2517-6161.1995.tb02031.x
- Bertram, J. E. A. and Biewener, A. A.** (1988). Bone curvature: sacrificing strength for load predictability? *J. Theor. Biol.* **131**, 75–92. doi:10.1016/S0022-5193(88)80122-X
- Biewener, A. A. and Daley, M. A.** (2007). Unsteady locomotion: integrating muscle function with whole body dynamics and neuromuscular control. *J. Exp. Biol.* **210**, 2949–2960. doi:10.1242/jeb.005801
- Bilo, D., Jahner, A. and Nachtigall, W.** (1980). Structure and innervation of wing muscle spindles in the domestic pigeon (*Columba livia* var. *domestica*); a light microscopical study. *Zool. J. Anat.* **103**, 41–61.
- Bishop, P. J., Graham, D. F., Lamas, L. P., Hutchinson, J. R., Rubenson, J., Hancock, J. A., Wilson, R. S., Hocknull, S. A., Barrett, R. S., Lloyd, D. G. et al.** (2018). The influence of speed and size on avian terrestrial locomotor biomechanics: predicting locomotion in extinct theropod dinosaurs. *PLoS ONE* **13**, e0192172. doi:10.1371/journal.pone.0192172
- Blob, R. W., Espinoza, N. R., Butcher, M. T., Lee, A. H., D'Amico, A. R., Baig, F. and Sheffield, K. M.** (2014). Diversity of limb-bone safety factors for locomotion in terrestrial vertebrates: evolution and mixed chains. *Integr. Comp. Biol.* **54**, 1058–1071. doi:10.1093/icb/ictu032
- Boettiger, C., Coop, G. and Ralph, P.** (2012). Is your phylogeny informative? measuring the power of comparative methods. *Evolution* **66**, 2240–2251. doi:10.1111/j.1558-5646.2011.01574.x
- Boggs, D. F.** (2002). Interactions between locomotion and ventilation in tetrapods. *Comp. Biochem. Physiol. A. Mol. Integr. Physiol.* **133**, 269–288. doi:10.1016/S1095-6433(02)00160-5
- Burnham, K. P. and Anderson, D. R.** (2001). Kullback–Leibler information as a basis for strong inference in ecological studies. *Wildl. Res.* **28**, 111–119. doi:10.1071/WR99107
- Butcher, M. T. and Blob, R. W.** (2008). Mechanics of limb bone loading during terrestrial locomotion in river cooter turtles (*Pseudemys concinna*). *J. Exp. Biol.* **211**, 1186–1186. doi:10.1242/jeb.021329
- Butcher, M. T., White, B. J., Hudzik, N. B., Gosnell, W. C., Parrish, J. H. A. and Blob, R. W.** (2011). *In vivo* strains in the femur of the Virginia opossum (*Didelphis virginiana*) during terrestrial locomotion: testing hypotheses of evolutionary shifts in mammalian bone loading and design. *J. Exp. Biol.* **214**, 2631–2640. doi:10.1242/jeb.049544
- Butler, A. B. and Hodos, W.** (2005). *Comparative Vertebrate Neuroanatomy: Evolution and Adaptation*. John Wiley & Sons.
- Carrier, D. R. and Farmer, C. G.** (2000). The integration of ventilation and locomotion in archosaurs. *Am. Zool.* **40**, 87–100. doi:10.1093/icb/40.1.87
- Clavel, J., Escarguel, G. and Merceron, G.** (2015). mvMORPH: an R package for fitting multivariate evolutionary models to morphometric data. *Methods Ecol. Evol.* **6**, 1311–1319. doi:10.1111/2041-210X.12420
- Cooper, N., Thomas, G. H., Venditti, C., Meade, A. and Freckleton, R. P.** (2016). A cautionary note on the use of Ornstein Uhlenbeck models in macroevolutionary studies. *Biol. J. Linn. Soc. Linn. Soc. Lond.* **118**, 64–77. doi:10.1111/bj.12701
- Crago, P. E., Houk, J. C. and Rymer, W. Z.** (1982). Sampling of total muscle force by tendon organs. *J. Neurophysiol.* **47**, 1069–1083. doi:10.1152/jn.1982.47.6.1069

- Cressler, C. E., Butler, M. A. and King, A. A. (2015). Detecting adaptive evolution in phylogenetic comparative analysis using the Ornstein-Uhlenbeck model. *Syst. Biol.* **64**, 953-968. doi:10.1093/sysbio/syv043
- Daley, M. A., Usherwood, J. R., Felix, G. and Biewener, A. A. (2006). Running over rough terrain: guinea fowl maintain dynamic stability despite a large unexpected change in substrate height. *J. Exp. Biol.* **209**, 171-187. doi:10.1242/jeb.01986
- Daley, M. A., Channon, A. J., Nolan, G. S. and Hall, J. (2016). Preferred gait and walk-run transition speeds in ostriches measured using GPS-IMU sensors. *J. Exp. Biol.* **219**, 3301-3308. doi:10.1242/jeb.142588
- Demes, B., Larson, S. G., Stern, J. T., Jungers, W. L., Biknevicius, A. R. and Schmitt, D. (1994). The kinetics of primate quadrupedalism: "hindlimb drive" reconsidered. *J. Hum. Evol.* **26**, 353-374. doi:10.1006/jhev.1994.1023
- Drew, T., Jiang, W. and Widajewicz, W. (2002). Contributions of the motor cortex to the control of the hindlimbs during locomotion in the cat. *Brain Res. Rev.* **40**, 178-191. doi:10.1016/S0165-0173(02)00200-X
- Drew, T., Prentice, S. and Schepens, B. (2004). Cortical and brainstem control of locomotion. *Prog. Brain Res.* **143**, 251-261. doi:10.1016/S0079-6123(03)43025-2
- English, A. W. (1989). Interlimb coordination during locomotion. *Integr. Comp. Biol.* **29**, 255-266. doi:10.1093/icb/29.1.255
- Fabre, A.-C., Granatosky, M. C., Hanna, J. B. and Schmitt, D. (2016). Coevolution between forelimb shape and loading regime in strepsirrhines. *Anat. Rec.* **S299**, 154.
- Felsenstein, J. (1985). Phylogenies and the comparative method. *Am. Nat.* **125**, 1-15. doi:10.1086/284325
- Fortier, P. A., Smith, A. M. and Rossignol, S. (1987). Locomotor deficits in the mutant mouse, Lurcher. *Exp. Brain Res.* **66**, 271-286. doi:10.1007/BF00243304
- Full, R. J., Kubow, T., Schmitt, J., Holmes, P. and Koditschek, D. (2002). Quantifying dynamic stability and maneuverability in legged locomotion. *Integr. Comp. Biol.* **42**, 149-157. doi:10.1093/icb/42.1.149
- Garland, T., Harvey, P. H. and Ives, A. R. (1992). Procedures for the analysis of comparative data using phylogenetically independent contrasts. *Syst. Biol.* **41**, 18-32. doi:10.1093/sysbio/41.1.18
- Gintof, C., Konow, N., Ross, C. F. and Sanford, C. P. J. (2010). Rhythmic chewing with oral jaws in teleost fishes: a comparison with amniotes. *J. Exp. Biol.* **213**, 1868-1875. doi:10.1242/jeb.041012
- Gosnell, W. C., Butcher, M. T., Maie, T. and Blob, R. W. (2011). Femoral loading mechanics in the Virginia opossum, *Didelphis virginiana*: torsion and mediolateral bending in mammalian locomotion. *J. Exp. Biol.* **214**, 3455-3466. doi:10.1242/jeb.060178
- Granatosky, M. C. (2015). Kinetic and kinematic patterns of arm-swinging in the red-shanked douc langur (*Pygathrix nemaeus*). *J. Vietnam. Primatol.* **2**, 33-40.
- Granatosky, M. C. (2018). Forelimb and hindlimb loading patterns during quadrupedal locomotion in the large flying fox (*Pteropus vampyrus*) and common vampire bat (*Desmodus rotundus*). *J. Zool.* **305**, 63-72. doi:10.1111/jzo.12538
- Granatosky, M. C. and Schmitt, D. (2019). The mechanical origins of arm-swinging. *J. Hum. Evol.* **130**, 61-71. doi:10.1016/j.jhev.2019.02.001
- Granatosky, M. C., Tripp, C. H. and Schmitt, D. (2016). Gait kinetics of above- and below-branch quadrupedal locomotion in lemurid primates. *J. Exp. Biol.* **219**, 53-63. doi:10.1242/jeb.120840
- Granatosky, M. C., Bryce, C. M., Hanna, J., Fitzsimons, A., Laird, M. F., Stilson, K., Wall, C. E. and Ross, C. F. (2018a). Inter-stride variability triggers gait transitions in mammals and birds. *Proc. R. Soc. B* **285**. doi:10.1098/rspb.2018.1766
- Granatosky, M. C., Fitzsimons, A., Zeininger, A. and Schmitt, D. (2018b). Mechanisms for the functional differentiation of the propulsive and braking roles of the forelimbs and hindlimbs during quadrupedal walking in primates and felines. *J. Exp. Biol.* **221**, 1-11. doi:10.1242/jeb.162917
- Gray, J. (1944). Studies in the mechanics of the tetrapod skeleton. *J. Exp. Biol.* **20**, 88-116.
- Gray, J. (1968). *Animal Locomotion*. London: William Clowes and Sons.
- Gregory, J. E. and Prosko, U. (1975). Responses of tendon organs in a lizard. *J. Physiol.* **248**, 519-529. doi:10.1113/jphysiol.1975.sp010986
- Gregory, J. E., Brockett, C. L., Morgan, D. L., Whitehead, N. P. and Prosko, U. (2002). Effect of eccentric muscle contractions on Golgi tendon organ responses to passive and active tension in the cat. *J. Physiol.* **538**, 209-218. doi:10.1113/jphysiol.2001.012785
- Grillner, S. (1975). Locomotion in vertebrates: central mechanisms and reflex interaction. *Physiol. Rev.* **55**, 247-304. doi:10.1152/physrev.1975.55.2.247
- Grillner, S. and Zangger, P. (1979). On the central generation of locomotion in the low spinal cat. *Exp. Brain Res.* **34**, 241-261. doi:10.1007/BF00235671
- Grillner, S. and Zangger, P. (1984). The effect of dorsal root transection on the efferent motor pattern in the cat's hindlimb during locomotion. *Acta Physiol. Scand.* **120**, 393-405. doi:10.1111/j.1748-1716.1984.tb07400.x
- Haiden, G. J. and Awad, E. A. (1981). The ultrastructure of the avian Golgi tendon organ. *Anat. Rec.* **200**, 153-161. doi:10.1002/ar.1092000205
- Hansen, T. F. (1997). Stabilizing selection and the comparative analysis of adaptation. *Evolution* **51**, 1341-1351. doi:10.1111/j.1558-5646.1997.tb01457.x
- Hedges, S. B., Dudley, J. and Kumar, S. (2006). TimeTree: a public knowledge-base of divergence times among organisms. *Bioinform. Oxf. Engl.* **22**, 2971-2972. doi:10.1093/bioinformatics/btl505
- Hedges, S. B., Marin, J., Suleski, M., Paymer, M. and Kumar, S. (2015). Tree of life reveals clock-like speciation and diversification. *Mol. Biol. Evol.* **32**, 835-845. doi:10.1093/molbev/msv037
- Hiimeae, K. M. and Palmer, J. B. (2003). Tongue movements in feeding and speech. *Crit. Rev. Oral Biol. Med.* **14**, 413-429. doi:10.1177/154411130301400604
- Hiimeae, K. M., Hayenga, S. M. and Reese, A. (1995). Patterns of tongue and jaw movement in a cinefluorographic study of feeding in the macaque. *Arch. Oral Biol.* **40**, 229-246. doi:10.1016/0003-9969(95)98812-D
- Ho, L. S. and Ané, C. (2014). A linear-time algorithm for Gaussian and non-Gaussian trait evolution models. *Syst. Biol.* **63**, 397-408. doi:10.1093/sysbio/syu005
- Horcholle-Bossavit, G., Jami, L., Petit, J., Vejsada, R. and Zytnicki, D. (1990). Ensemble discharge from Golgi tendon organs of cat peroneus tertius muscle. *J. Neurophysiol.* **64**, 813-821. doi:10.1152/jn.1990.64.3.813
- Houk, J. and Henneman, E. (1967). Responses of Golgi tendon organs to active contractions of the soleus muscle of the cat. *J. Neurophysiol.* **30**, 466-481. doi:10.1152/jn.1967.30.3.466
- Huber, G. C. and Dewitt, L. M. (1900). A contribution on the nerve terminations in neuro-tendinous end-organs. *J. Comp. Neurol.* **10**, 159-208. doi:10.1002/cne.910100204
- Hulliger, M. (1984). The mammalian muscle spindle and its central control. In *Reviews of Physiology, Biochemistry and Pharmacology* (ed. E. Cordat, D. Barber, J. Leipziger, L. Pardo, C. Stock, N. Schmitt and M. E. O'Donnell), Vol. 101, pp. 1-110. Springer.
- Ichise, T., Kano, M., Hashimoto, K., Yanagihara, D., Nakao, K., Shigemoto, R., Katsuki, M. and Aiba, A. (2000). mGluR1 in cerebellar Purkinje cells essential for long-term depression, synapse elimination, and motor coordination. *Science* **288**, 1832-1835. doi:10.1126/science.288.5472.1832
- Ives, A. R., Midford, P. E. and Garland, T. (2007). Within-species variation and measurement error in phylogenetic comparative methods. *Syst. Biol.* **56**, 252-270. doi:10.1080/10635150701313830
- James, N. T. and Meek, G. A. (1973). An electron microscopical study of avian muscle spindles. *J. Ultrastruct. Res.* **43**, 193-204. doi:10.1016/S0022-5320(73)80032-2
- Jedrzejewski, W., Schmidt, K., Theuerkauf, J., Jedrzejewska, B. and Okarma, H. (2001). Daily movements and territory use by radio-collared wolves (*Canis lupus*) in Białowieża Primeval Forest in Poland. *Can. J. Zool.* **79**, 1993-2004. doi:10.1139/z01-147
- Jetz, W. and Pyron, R. A. (2018). The interplay of past diversification and evolutionary isolation with present imperilment across the amphibian tree of life. *Nat. Ecol. Evol.* **2**, 850. doi:10.1038/s41559-018-0515-5
- Jetz, W., Thomas, G. H., Joy, J. B., Redding, D. W., Hartmann, K. and Mooers, A. O. (2014). Global distribution and conservation of evolutionary distinctness in birds. *Curr. Biol. CB* **24**, 919-930. doi:10.1016/j.cub.2014.03.011
- Johansson, H. (1988). Rubrospinal and rubrobulbosplinal influences on dynamic and static γ -motoneurons. *Behav. Brain Res.* **28**, 97-107. doi:10.1016/0166-4328(88)90084-8
- Jordan, K., Challis, J. H. and Newell, K. M. (2007). Walking speed influences on gait cycle variability. *Gait Posture* **26**, 128-134. doi:10.1016/j.gaitpost.2006.08.010
- Karakasiliotis, K., Thandiackal, R., Melo, K., Horvat, T., Mahabadi, N. K., Tsitkov, S., Cabelguen, J. M. and Ijspeert, A. J. (2016). From cineradiography to biorobots: an approach for designing robots to emulate and study animal locomotion. *J. R. Soc. Interface* **13**, 20151089. doi:10.1098/rsif.2015.1089
- Keene, O. N. (1995). The log transformation is special. *Stat. Med.* **14**, 811-819. doi:10.1002/sim.4780140810
- Kilbourne, B. M., Andrada, E., Fischer, M. S. and Nyakatura, J. A. (2016). Morphology and motion: hindlimb proportions and swing phase kinematics in terrestrially locomoting charadriiform birds. *J. Exp. Biol.* **219**, 1405-1416. doi:10.1242/jeb.124081
- Klaassen, R. H. G., Strandberg, R., Hake, M. and Alerstam, T. (2008). Flexibility in daily travel routines causes regional variation in bird migration speed. *Behav. Ecol. Sociobiol.* **62**, 1427-1432. doi:10.1007/s00265-008-0572-x
- Knight, K. C. and Lee, D. (2019). Comparative biomechanics of horizontal, fine-branch locomotion in lizards: part 1. Society for Integrative and Comparative Biology Annual Meeting, Tampa, Florida, p. E125.
- Kram, R. and Taylor, C. R. (1990). Energetics of running: a new perspective. *Nature* **346**, 265. doi:10.1038/346265a0
- Kuhn, T. S., Mooers, A. Ø. and Thomas, G. H. (2011). A simple polytomy resolver for dated phylogenies. *Methods Ecol. Evol.* **2**, 427-436. doi:10.1111/j.2041-210X.2011.00103.x
- Kumar, S. and Hedges, S. B. (2011). TimeTree2: species divergence times on the iPhone. *Bioinform. Oxf. Engl.* **27**, 2023-2024. doi:10.1093/bioinformatics/btr315
- Kumar, S., Stecher, G., Suleski, M. and Hedges, S. B. (2017). TimeTree: a resource for timeliness, timetrees, and divergence times. *Mol. Biol. Evol.* **34**, 1812-1819. doi:10.1093/molbev/msx116
- Lowell, R. B. (1985). Selection for increased safety factors of biological structures as environmental unpredictability increases. *Science* **228**, 1009-1011. doi:10.1126/science.228.4702.1009
- Maier, A. (1992). The avian muscle spindle. *Anat. Embryol. (Berl.)* **186**, 1-25. doi:10.1007/BF00710398

- Marcus Rowcliffe, J., Carbone, C., Kays, R., Kranstauber, B. and Jansen, P. A. (2012). Bias in estimating animal travel distance: the effect of sampling frequency. *Methods Ecol. Evol.* **3**, 653-662. doi:10.1111/j.2041-210X.2012.00197.x
- Matthews, P. B. (1972). *Mammalian Muscle Receptors and their Central Actions*. Hodder & Stoughton Educational.
- McElroy, E. J., Wilson, R., Biknevicius, A. R. and Reilly, S. M. (2014). A comparative study of single-leg ground reaction forces in running lizards. *J. Exp. Biol.* **217**, 735-742. doi:10.1242/jeb.095620
- Mileusnic, M. P. and Loeb, G. E. (2009). Force estimation from ensembles of Golgi tendon organs. *J. Neural Eng.* **6**, 036001. doi:10.1088/1741-2560/6/3/036001
- Morton, S. M. and Bastian, A. J. (2006). Cerebellar contributions to locomotor adaptations during splitbelt treadmill walking. *J. Neurosci. Off. J. Soc. Neurosci.* **26**, 9107-9116. doi:10.1523/JNEUROSCI.2622-06.2006
- Munteanu, V., Diamond, K., Schneider, N., Riley, A., McKamy, A. and Blob, R. W. (2019). Effects of ecological transitions on locomotor morphology: do changes in bone loads have implications for limb elongation in arboreal tetrapods? Society for Integrative and Comparative Biology Annual Meeting, Tampa, Florida, p. E374.
- Nagy, K. A. (1987). Field metabolic rate and food requirement scaling in mammals and birds. *Ecol. Monogr.* **57**, 111-128. doi:10.2307/1942620
- Nagy, K. A. (2005). Field metabolic rate and body size. *J. Exp. Biol.* **208**, 1621-1625. doi:10.1242/jeb.01553
- Nagy, K. A., Girard, I. A. and Brown, T. K. (1999). Energetics of free-ranging mammals, reptiles, and birds. *Annu. Rev. Nutr.* **19**, 247-277. doi:10.1146/annurev.nutr.19.1.247
- Nassar, P. N., Jackson, A. C. and Carrier, D. R. (2001). Entraining the natural frequencies of running and breathing in guinea fowl (*Numida meleagris*). *J. Exp. Biol.* **204**, 1641-1651.
- Nyakatura, J. A., Andrada, E., Curth, S. and Fischer, M. S. (2014). Bridging "Romer's Gap": limb mechanics of an extant belly-dragging lizard inform debate on tetrapod locomotion during the early carboniferous. *Evol. Biol.* **41**, 175-190. doi:10.1007/s11692-013-9266-z
- Nyakatura, J. A., Melo, K., Horvat, T., Karakasiotis, K., Allen, V. R., Andikfar, A., Andrada, E., Arnold, P., Lauströer, J., Hutchinson, J. R. et al. (2019). Reverse-engineering the locomotion of a stem amniote. *Nature* **565**, 351. doi:10.1038/s41586-018-0851-2
- O'Connor, S. M., Xu, H. Z. and Kuo, A. D. (2012). Energetic cost of walking with increased step variability. *Gait Posture* **36**, 102-107. doi:10.1016/j.gaitpost.2012.01.014
- Ovalle, W. K. (1976). Fine structure of the avian muscle spindle capsule. *Cell Tissue Res.* **166**, 285-298. doi:10.1007/BF00220126
- Palmer, J. B., Hiimeae, K. M. and Liu, J. (1997). Tongue-jaw linkages in human feeding: a preliminary videofluorographic study. *Arch. Oral Biol.* **42**, 429-441. doi:10.1016/S0003-9969(97)00020-4
- Paradis, E., Claude, J. and Strimmer, K. (2004). APE: analyses of phylogenetics and evolution in R language. *Bioinformatics* **20**, 289-290. doi:10.1093/bioinformatics/btg412
- Pearson, K. G., Misiaszek, J. E. and Fouad, K. (1998). Enhancement and resetting of locomotor activity by muscle afferents. *Ann. N. Y. Acad. Sci.* **860**, 203-215. doi:10.1111/j.1749-6632.1998.tb09050.x
- Pontzer, H. (2016). A unified theory for the energy cost of legged locomotion. *Biol. Lett.* **12**, 20150935. doi:10.1098/rsbl.2015.0935
- Prochazka, A., Gritsenko, V. and Yakovenko, S. (2002). Sensory control of locomotion: reflexes versus higher-level control. In *Sensorimotor Control of Movement and Posture* (ed. S. C. Gandevia, U. Proske and D. G. Stuart), pp. 357-367. Springer.
- Proske, U. (1979). The Golgi tendon organ. *Trends Neurosci.* **2**, 7-8. doi:10.1016/0166-2236(79)90004-3
- Proske, U. (1997). The mammalian muscle spindle. *Physiology* **12**, 37-42. doi:10.1152/physiologyonline.1997.12.1.37
- Purves, D. A. and Fitzpatrick, G. (2001). *Neuroscience*. Sunderland, MA: Sinauer Associates Inc.
- Reilly, S. M., McElroy, E. J. and Biknevicius, A. R. (2007). Posture, gait and the ecological relevance of locomotor costs and energy-saving mechanisms in tetrapods. *Zoology* **110**, 271-289. doi:10.1016/j.zool.2007.01.003
- Revell, L. J. (2012). phytools: an R package for phylogenetic comparative biology (and other things). *Methods Ecol. Evol.* **3**, 217-223. doi:10.1111/j.2041-210X.2011.00169.x
- Riemann, B. L. and Lephart, S. M. (2002). The sensorimotor system, part II: the role of proprioception in motor control and functional joint stability. *J. Athl. Train.* **37**, 80.
- Romanovsky, D., Moseley, A. E., Mrak, R. E., Taylor, M. D. and Dobretsov, M. (2007). Phylogenetic preservation of $\alpha 3$ Na⁺, K⁺-ATPase distribution in vertebrate peripheral nervous systems. *J. Comp. Neurol.* **500**, 1106-1116. doi:10.1002/cne.21218
- Roquet, C., Lavergne, S. and Thuiller, W. (2014). One tree to link them all: a phylogenetic dataset for the European tetrapoda. *PLoS Curr.* **6**. doi:10.1371/currents.tol.5102670fff8aa5c918e78f5592790e48
- Ross, C. F., Eckhardt, A., Herrel, A., Hylander, W. L., Metzger, K. A., Schaeerlaeken, V., Washington, R. L. and Williams, S. H. (2007). Modulation of intra-oral processing in mammals and lepidosaurs. *Integr. Comp. Biol.* **47**, 118-136. doi:10.1093/icb/icm044
- Ross, C. F., Baden, A. L., Georgi, J., Herrel, A., Metzger, K. A., Reed, D. A., Schaeerlaeken, V. and Wolff, M. S. (2010). Chewing variation in lepidosaurs and primates. *J. Exp. Biol.* **213**, 572-584. doi:10.1242/jeb.036822
- Ross, C. F., Blob, R. W., Carrier, D. R., Daley, M. A., Deban, S. M., Demes, B., Gripper, J. L., Iriarte-Diaz, J., Kilbourne, B. M., Landberg, T. et al. (2013). The evolution of locomotor rhythmicity in tetrapods. *Evolution* **67**, 1209-1217. doi:10.1111/evo.12015
- Schliep, K. P. (2011). phangorn: phylogenetic analysis in R. *Bioinforma. Oxf. Engl.* **27**, 592-593. doi:10.1093/bioinformatics/btq706
- Schmitt, D. (1999). Compliant walking in primates. *J. Zool.* **248**, 149-160. doi:10.1111/j.1469-7998.1999.tb01191.x
- Schmitt, D. and Hanna, J. B. (2004). Substrate alters forelimb to hindlimb peak force ratios in primates. *J. Hum. Evol.* **46**, 237-252. doi:10.1016/j.jhevol.2003.11.008
- Schmitz, L. and Higham, T. E. (2018). Non-uniform evolutionary response of gecko eye size to changes in diel activity patterns. *Biol. Lett.* **14**, 20180064. doi:10.1098/rsbl.2018.0064
- Serrien, D. J., Li, Y., Steyvers, M., Debaere, F. and Swinnen, S. P. (2001). Proprioceptive regulation of interlimb behavior: interference between passive movement and active coordination dynamics. *Exp. Brain Res.* **140**, 411-419. doi:10.1007/s002210100820
- Sheffield, K. M. and Blob, R. W. (2011). Loading mechanics of the femur in tiger salamanders (*Ambystoma tigrinum*) during terrestrial locomotion. *J. Exp. Biol.* **214**, 2603-2615. doi:10.1242/jeb.048736
- Sheffield, K. M., Butcher, M. T., Shugart, S. K., Gander, J. C. and Blob, R. W. (2011). Locomotor loading mechanics in the hindlimbs of tegu lizards (*Tupinambis merianae*): comparative and evolutionary implications. *J. Exp. Biol.* **214**, 2616-2630. doi:10.1242/jeb.048801
- Shneider, N. A., Brown, M. N., Smith, C. A., Pickel, J. and Alvarez, F. J. (2009). Gamma motor neurons express distinct genetic markers at birth and require muscle spindle-derived GDNF for postnatal survival. *Neural Develop.* **4**, 42. doi:10.1186/1749-8104-4-42
- Sokal, R. R. and Rohlf, F. J. (2012). *Biometry: the Principles and Practice of Statistics in Biological Research*, 6th edn. New York: Freeman & Company.
- Stark, R. C., Fox, S. F. and Leslie, D. M., Jr (2005). Male Texas horned lizards increase daily movements and area covered in spring: a mate searching strategy? *J. Herpetol.* **39**, 169-173. doi:10.1670/0022-1511(2005)039[0168:MTHLID]2.0.CO;2
- Taylor, C. R., Heglund, N. C., McMahon, T. A. and Looney, T. R. (1980). Energetic cost of generating muscular force during running: a comparison of large and small animals. *J. Exp. Biol.* **86**, 9-18.
- Taylor, C. R., Heglund, N. C. and Maloiy, G. M. (1982). Energetics and mechanics of terrestrial locomotion. I. Metabolic energy consumption as a function of speed and body size in birds and mammals. *J. Exp. Biol.* **97**, 1-21. doi:10.1146/annurev.ph.44.030182.000525
- ten Donkelaar, H. J. (1988). Evolution of the red nucleus and rubrospinal tract. *Behav. Brain Res.* **28**, 9-20. doi:10.1016/0166-4328(88)90072-1
- Thompson, G. (1992). Daily distance travelled and foraging areas of Varanus gouldii (Reptilia: Varanidae) in a semi-urban environment. *Wildl. Res.* **19**, 743-753. doi:10.1071/WR9920743
- Thompson, G. G., De Boer, M. and Pianka, E. R. (1999). Activity areas and daily movements of an arboreal monitor lizard, *Varanus tristis* (Squamata: Varanidae) during the breeding season. *Aust. J. Ecol.* **24**, 117-122. doi:10.1046/j.1442-9993.1999.241952.x
- Tonini, J. F. R., Beard, K. H., Ferreira, R. B., Jetz, W. and Pyron, R. A. (2016). Fully-sampled phylogenies of squamates reveal evolutionary patterns in threat status. *Biol. Conserv.* **204**, 23-31. doi:10.1016/j.biocon.2016.03.039
- Verdaasdonk, B. W., Koopman, H. F. J. M. and Helm, F. C. T. V. D. (2006). Energy efficient and robust rhythmic limb movement by central pattern generators. *Neural Netw.* **19**, 388-400. doi:10.1016/j.neunet.2005.09.003
- Wetzel, M. C., Atwater, A. E., Wait, J. V. and Stuart, D. G. (1976). Kinematics of locomotion by cats with a single hindlimb deafferented. *J. Neurophysiol.* **39**, 667-678. doi:10.1152/jn.1976.39.4.667
- Wild, J. M. and Williams, M. N. (2000). Rostral wulst in passerine birds. I. Origin, course, and terminations of an avian pyramidal tract. *J. Comp. Neurol.* **416**, 429-450. doi:10.1002/(SICI)1096-9861(20000124)416:4<429::AID-CNE2>3.0.CO;2-X
- Winter, B. (2013). Linear models and linear mixed effects models in R with linguistic applications. arXiv:1308.5499
- Yanagihara, D., Udo, M., Kondo, I. and Yoshida, T. (1993). A new learning paradigm: adaptive changes in interlimb coordination during perturbed locomotion in decerebrate cats. *Neurosci. Res.* **18**, 241-244. doi:10.1016/0168-0102(93)90060-4

Table S1. Statistical parameters derived from linear mixed-effects models demonstrating the statistical importance of various fixed effects. Values in bold illustrate fixed effects that significantly influence each respective response variable.

Response variable	Fixed effect	Estimate	Standard Error	<i>t</i> value	<i>F</i> value	<i>P</i> value
Peak braking force <i>CV</i> *	(Intercept)	1.28	0.17	-	-	-
	Golgi tendon organ morphology	0.58	0.09	6.56	37.19	< 0.001
	Substrate	0.27	0.08	3.43	10.24	0.002
	Dimensionless speed	-0.04	0.14	-0.27	0.02	0.892
	Count	0.00	0.00	1.26	1.71	0.195
	Dimensionless speed <i>CV</i> *	0.12	0.07	1.71	2.41	0.123
	Mass	-0.08	0.05	-1.55	2.16	0.148
Peak propulsive force <i>CV</i> *	Contact time	0.13	0.19	0.69	0.49	0.485
	(Intercept)	1.11	0.14	-	-	-
	Golgi tendon organ morphology	0.44	0.08	5.45	29.72	< 0.001
	Substrate	0.10	0.07	1.37	1.87	0.178
	Dimensionless speed	0.00	0.13	0.03	0.00	0.979
	Count	0.00	0.00	1.72	2.97	0.088
	Dimensionless speed <i>CV</i> *	0.15	0.05	2.78	7.72	0.006
Peak medial force <i>CV</i> *	Mass	-0.05	0.04	-1.03	1.07	0.306
	Contact time	-0.02	0.17	-0.11	0.01	0.910
	(Intercept)	1.53	0.16	-	-	-
	Golgi tendon organ morphology	0.24	0.08	2.96	8.74	0.005
	Substrate	-0.07	0.07	-0.95	0.90	0.349
	Dimensionless speed	0.07	0.13	0.53	0.28	0.597
	Count	0.01	0.00	3.08	9.50	0.003
Peak lateral force <i>CV</i> *	Dimensionless speed <i>CV</i> *	0.07	0.06	1.18	1.38	0.241
	Mass	0.06	0.05	1.23	1.50	0.227
	Contact time	0.16	0.18	0.91	0.82	0.370
	(Intercept)	1.59	0.14	-	-	-
	Golgi tendon organ morphology	0.16	0.08	2.04	4.17	0.047

	Substrate	0.32	0.07	4.74	22.49	< 0.001
	Dimensionless speed	0.25	0.12	2.05	4.20	0.046
	Count	0.01	0.00	2.94	8.66	0.004
	Dimensionless speed <i>CV</i> *	0.03	0.06	0.59	0.35	0.555
	Mass	-0.09	0.05	-1.90	3.60	0.063
	Contact time	0.38	0.16	2.35	5.52	0.022
	(Intercept)	0.72	0.15	-	-	-
Peak vertical force <i>CV</i> *	Golgi tendon organ morphology	0.24	0.09	2.56	6.57	0.014
	Substrate	-0.12	0.08	-1.48	2.18	0.147
	Dimensionless speed	0.11	0.14	0.75	0.56	0.458
	Count	0.00	0.00	1.59	2.54	0.114
	Dimensionless speed <i>CV</i> *	0.26	0.05	4.77	22.72	< 0.001
	Mass	-0.04	0.05	-0.83	0.68	0.413
	Contact time	-0.10	0.19	-0.51	0.26	0.609
Timing of peak braking force <i>CV</i> *	(Intercept)	1.43	0.12	-	-	-
	Golgi tendon organ morphology	0.33	0.08	4.39	19.27	< 0.001
	Substrate	0.17	0.07	2.49	6.22	0.016
	Dimensionless speed	-0.06	0.11	-0.57	0.32	0.573
	Count	0.00	0.00	0.69	0.48	0.491
	Dimensionless speed <i>CV</i> *	0.09	0.04	2.17	4.70	0.032
	Mass	-0.14	0.04	-3.17	10.08	0.002
Contact time	0.24	0.15	1.59	2.52	0.116	
Timing of braking to propulsive transition <i>CV</i> *	(Intercept)	1.12	0.12	-	-	-
	Golgi tendon organ morphology	0.39	0.07	5.49	27.62	< 0.001
	Substrate	0.40	0.06	6.25	34.45	< 0.001
	Dimensionless speed	-0.19	0.11	-1.73	2.67	0.11
	Count	0.00	0.00	0.48	0.29	0.59
	Dimensionless speed <i>CV</i> *	0.05	0.04	1.26	1.77	0.19
	Mass	-0.17	0.04	-4.03	13.81	< 0.001
Contact time	0.09	0.15	-0.61	0.28	0.60	
Timing of peak	(Intercept)	0.78	0.13	-	-	-
	Golgi tendon organ morphology	0.40	0.07	5.84	34.09	< 0.001

propulsive force CV*	Substrate	0.35	0.06	5.84	34.05	< 0.001
	Dimensionless speed	-0.19	0.11	-1.78	3.16	0.083
	Count	0.00	0.00	-0.27	0.07	0.788
	Dimensionless speed CV*	0.14	0.05	2.69	7.25	0.008
	Mass	-0.12	0.04	-2.94	8.66	0.005
	Contact time	0.05	0.15	0.36	0.13	0.722
Timing of peak medial force CV*	(Intercept)	1.80	0.16	-	-	-
	Golgi tendon organ morphology	0.22	0.10	2.31	5.32	0.025
	Substrate	0.03	0.09	0.33	0.11	0.743
	Dimensionless speed	-0.06	0.15	-0.43	0.19	0.668
	Count	0.00	0.00	0.98	0.96	0.329
	Dimensionless speed CV*	-0.11	0.06	-1.88	3.53	0.062
	Mass	0.02	0.06	0.30	0.09	0.762
	Contact time	0.01	0.20	0.04	0.00	0.967
Timing of peak lateral force CV*	(Intercept)	1.97	0.12	-	-	-
	Golgi tendon organ morphology	-0.10	0.06	-1.75	3.06	0.087
	Substrate	0.33	0.05	6.24	38.95	< 0.001
	Dimensionless speed	0.07	0.09	0.79	0.63	0.433
	Count	0.00	0.00	2.53	6.38	0.015
	Dimensionless speed CV*	-0.13	0.05	-2.72	7.42	0.007
	Mass	-0.07	0.04	-1.85	3.42	0.071
	Contact time	0.48	0.13	3.77	14.20	< 0.001
Timing of peak vertical force CV*	(Intercept)	1.59	0.15	-	-	-
	Golgi tendon organ morphology	0.01	0.09	0.13	0.02	0.896
	Substrate	-0.09	0.08	-1.11	1.23	0.273
	Dimensionless speed	0.06	0.14	0.41	0.17	0.682
	Count	0.00	0.00	1.09	1.18	0.280
	Dimensionless speed CV*	-0.03	0.05	-0.60	0.36	0.547
	Mass	-0.13	0.05	-2.56	6.53	0.013
	Contact time	0.24	0.18	1.36	1.84	0.179

Information not pertinent.

Table S2: Evolutionary models fit to log₁₀ limb loading and stride cycle CV* with intraspecific sampling included in the model. Bolded models have the most support. Values presented are mean ± standard deviation based on running the analysis on 100 trees to account for phylogenetic uncertainty. Variables defined as follows: σ^2 = Brownian motion rate parameter, α = strength of pull towards trait optimum under OU model, $T_{1/2}$ = phylogenetic half-life, θ = trait optima. Models as follows: BM1 = single rate Brownian motion, BM-M = two rate Brownian motion, OU-1 = single optimum Ornstein-Uhlenbeck, OU-M = two optima Ornstein-Uhlenbeck.

Variable	Model	σ	α	$T_{1/2}$	θ	Akaike's information criterion	Akaike Weights
Peak braking force CV*	BM1	1.7e-04±6.4e-07			1.5±0.00	78.1±0.02	0.21±0.00
	BM-M	1.5e-11±3.1e-11 5.0e-04±2.9e-06			1.7±0.00	77.1±0.04	0.34±0.00
	OU-1	6.0e-04±2.6e-06	0.0077±0.00003	90	1.5±0.00	79.0±0.03	0.13±0.00
	OU-M	3.9e-04±2.1e-06	0.0110±0.00005	63	1.7±0.00 1.2±0.00	77.2±0.01	0.32±0.00
Peak propulsive force CV*	BM1	9.5e-19±9.4e-18			1.5±0.00	48.3±0.00	0.56±0.00
	BM-M	1.7e-16±6.6e-16 1.9e-15±1.1e-14			1.5±0.00	50.5±0.00	0.18±0.00
	OU-1	5.3e-21±5.7e-21	0.0084±0.00002	83	1.5±0.00	50.5±0.00	0.18±0.00
	OU-M	3.4e-13±9.4e-13	1.2e-8±1.6e-8	5.8e7	1.5±0.00, 1.4e5±2.0e5	52.4±0.00	0.07±0.00
Peak medial force CV*	BM1	2.5e-19±1.7e-18			1.7±0.00	64.1±0.00	0.57±0.00
	BM-M	2.3e-15±6.9e-15 4.8e-15±1.0e-14			1.7±0.00	66.3±0.00	0.19±0.00
	OU-1	7.9e-22 ±1.6e-22	0.0073±6.0e-6	95	1.7±0.00	66.3±0.00	0.19±0.00
	OU-M	3.4e-12±7.6e-12	1.2e-8±1.8e-8	5.8e7	1.7±0.00 -3.1e5±3.8e+05	68.5±0.00	0.06±0.00
	BM1	3.7e-17 ± 3.6e-16			1.6±0.00	55.0±0.00	0.57±0.00

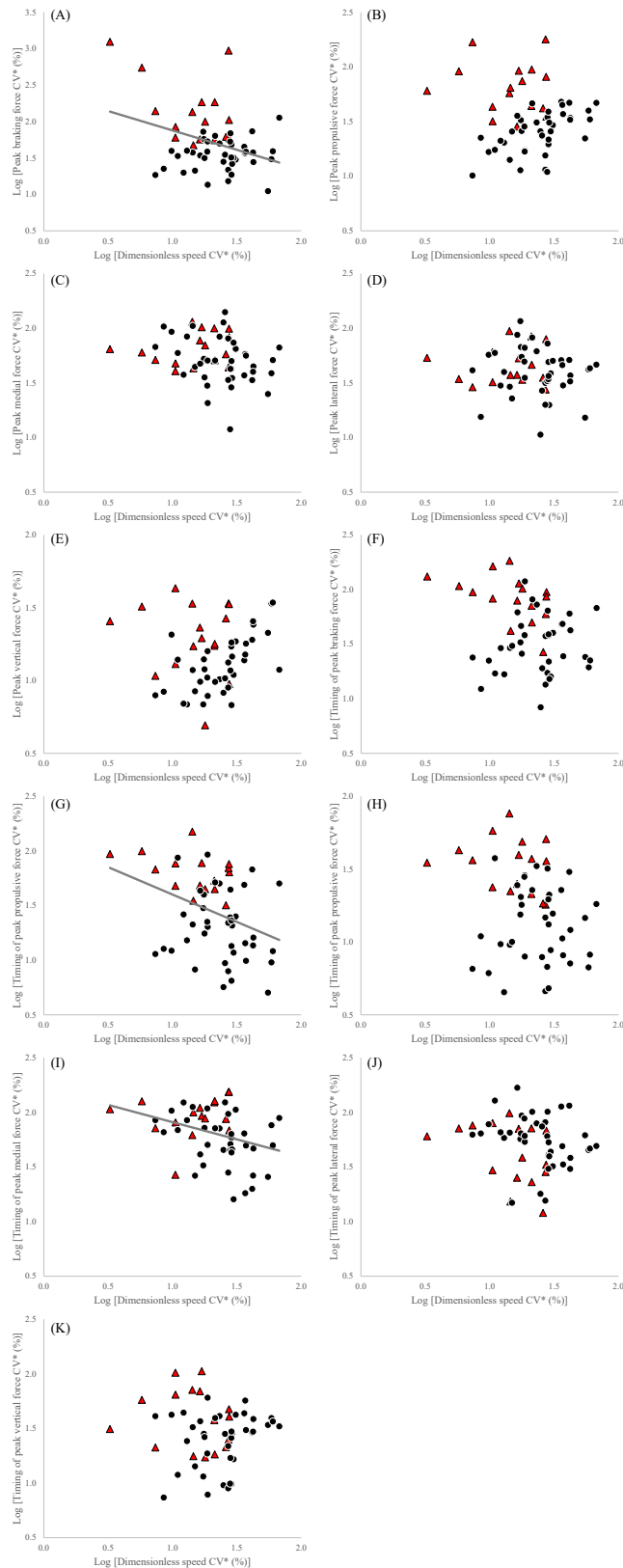
Peak lateral force CV*	BM-M	6.2e-16 ±2.3e-15 7.3e-16 ±1.8e-15			1.6±0.00	57.3±0.00	0.19±0.00
	OU-1	4.1e-20 ±2.9e-20	0.0074±3.8e-6	94	1.6±0.00	57.3±0.00	0.19±0.00
	OU-M	3.8e-13±2.1e-12	9.5e-9±8.7e-9	7.2e7	1.7±0.00, -1.9e5±2.2e5	59.5±0.00	0.06±0.00
Peak vertical force CV*	BM1	5.6e-05±4.3e-07			1.1±0.00	29.5±0.03	0.23±0.00
	BM-M	5.2e-12±9.5e-12 3.0e-04±3.6e-06			1.0±0.00	28.0±0.06	0.50±0.01
	OU-1	5.6e-05±3.2e-07	2.2e-6±3.8e-6	3.2e5	1.1±0.00	31.7±0.03	0.08±0.00
	OU-M	1.5e-10±2.3e-10	1.4e-8±2.5e-8	5.0e7	0.7±0.00, 1.7e6±1.9e6	29.9±0.00	0.19±0.00
Timing of peak braking force CV*	BM1	3.8e-05±2.1e-07			1.5±0.00	65.5±0.01	0.33±0.00
	BM-M	3.6e-13±1.7e-12 1.4e-04±4.9e-06			1.6±0.00	67.5±0.05	0.12±0.00
	OU-1	2.6e-04±8.4e-06	0.0099±0.150	70	1.5±0.00	67.1±0.02	0.15±0.00
	OU-M	2.1e-10±1.5e-09	0.0003±0.012	2.3e3	1.7±0.00, 1.4±0.00	65.1±0.00	0.40±0.00
Timing of braking to propulsive transition CV*	BM1	7.3e-05 ±7.7e-07			1.3±0.00	64.1±0.03	0.19±0.00
	BM-M	6.1e-05±5.0e-05 1.2e-04±1.2e-04			1.3±0.03	66.0±0.33	0.07±0.01
	OU-1	8.1e-02 ±1.8e-01	1.2±2.7	0.6	1.2±0.00	63.3±0.03	0.28±0.00
	OU-M	6.2e-02±1.3e-01	1.1±2.4	0.6	1.4±0.00, 1.2±0.00	62.3±0.01	0.45±0.01
Timing of peak propulsive force CV*	BM1	0.00057±1.6e-05			1.2±0.00	71.1±0.59	0.00±0.00
	BM-M	0.00009±3.1e-06 0.00097±3.6e-05			1.2±0.00	68.7±0.55	0.01±0.00
	OU-1	0.17000±3.1e-01	1.4±2.6	0.5	1.1±0.00	60.0±0.19	0.48±0.01
	OU-M	0.33000±8.3e-01	3.0±7.4	0.2	1.3±0.00, 1.1±0.00	59.9±0.15	0.51±0.01
Timing of peak medial force CV*	BM1	1.5e-19±1.4e-18			1.7±0.00	76.3±0.00	0.54±0.02
	BM-M	1.4e-11± 3.4e-11 1.1e-05± 1.0e-05			1.7±0.00	78.5±0.01	0.18±0.02
	OU-1	4.9e-18 ±8.1e-18	0.008±0.00001	87	1.7±0.00	78.5±0.00	0.18±0.00
	OU-M	3.2e-10±1.8e-09	0.120±0.018	6	1.8±0.00, 1.7±0.00	79.6±0.00	0.11±0.00

Timing of peak lateral force CV*	BM1	4.6e-05±8.1e-06			1.5±0.03	73.6±0.37	0.29±0.03
	BM-M	2.5e-11±5.3e-11 1.2e-04±6.7e-07			1.5±0.00	74.8±0.01	0.16±0.01
	OU-1	7.1e-04±4.8e-05	0.030±0.002	23	1.5±0.00	74.8±0.01	0.16±0.01
	OU-M	6.3e-04±6.4e-06	0.002±0.001	347	1.9±0.00, 1.5±0.00	73.0±0.00	0.39±0.02
Timing of peak vertical force CV*	BM1	3.1e-05±3.1e-07			1.3±0.00	52.3±0.02	0.52±0.00
	BM-M	7.8e-12 ±1.8e-11 1.3e-04 ±2.1e-06			1.3±0.00	53.7±0.07	0.25±0.00
	OU-1	5.6e-05±4.1e-06	0.0021±0.0003	330	1.3±0.00	54.5±0.03	0.17±0.00
	OU-M	5.6e-05±4.1e-06	0.0020±0.0003	347	1.3±0.00, 1.3±0.01	56.8±0.03	0.05±0.00
Stride cycle duration CV*	BM1	1.7e-04±1.3e-06			1.1±0.00	29.8±0.14	0.15±0.01
	BM-M	8.3e-05±8.0e-07 3.4e-04±4.0e-06			1.1±0.00	29.3±0.14	0.20±0.01
	OU-1	9.0e-04±6.8e-05	0.015±0.001	46	1.2±0.00	28.3±0.13	0.34±0.01
	OU-M	1.2e-03±1.3e-03	0.024±0.028	29	1.1±0.00, 1.2±0.00	28.5±0.14	0.30±0.01

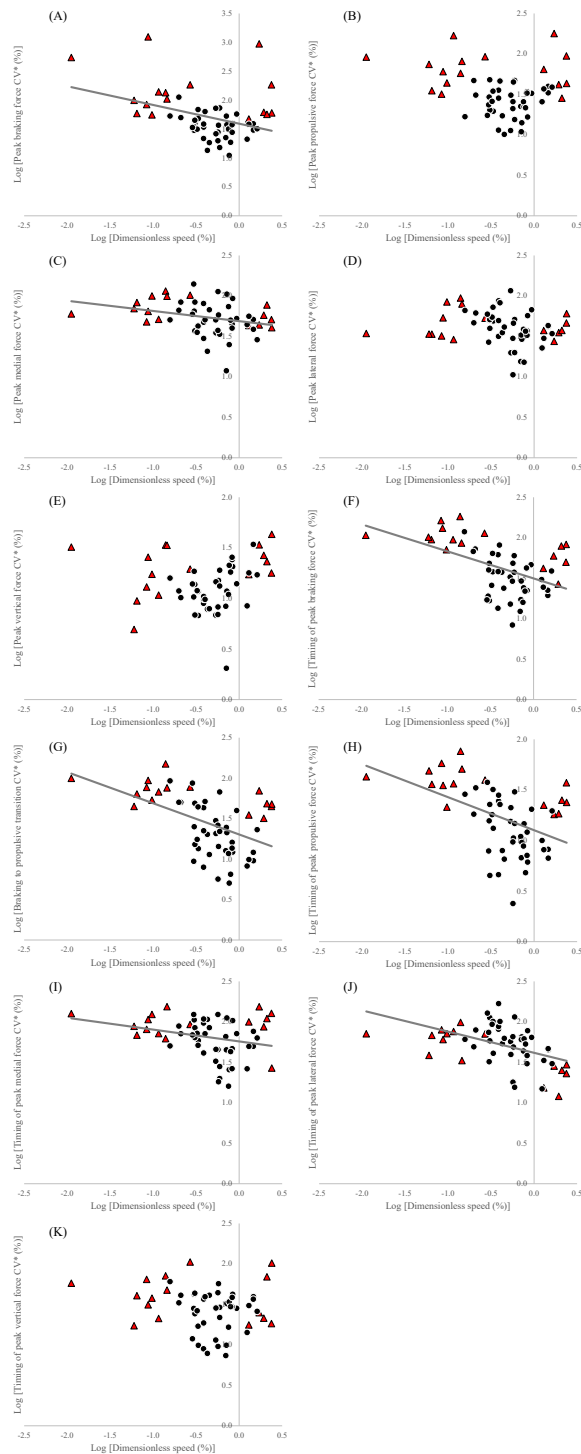
Table S3: Type I error and, statistical power computed from simulations based on the OU-M models fit to each variable. Selection opportunity (η), the discriminability ratio (ϕ) and the signal to noise ratio (SNR) were computed using equations from Cressler et al. (2015).

		Type I error	Power	η	ϕ	SNR
Raw with standard error included	Peak Brake	0.15	1.00	3.9E+00	1.9E+02	3.7E+02
	Peak Accel	0.17	1.00	4.2E-06	6.4E+13	1.3E+11
	Peak Vertical	0.05	1.00	3.3E-06	6.9E+13	1.3E+11
	Peak Lateral	0.1	1.00	4.2E-06	1.4E+13	2.9E+10
	Peak Medial	0.12	1.00	4.9E-06	1.9E+12	4.2E+09
	Time Brake	0.26	1.00	3.9E+02	4.8E+00	9.4E+01
	Time Accel	0.15	1.00	1.1E-01	3.5E+07	1.1E+07
	Time Vertical	0.22	1.00	7.0E-01	4.0E+01	3.4E+01
	Time Lateral	0.17	1.00	4.2E+01	1.5E+08	9.9E+08
	Time Medial	0.22	1.00	7.0E-01	0.0E+00	0.0E+00
	Time BP	0.13	1.00	1.1E+03	1.5E+00	4.8E+01
	Cycle	0.24	1.00	8.4E+00	1.8E+01	5.3E+01
Residual without standard error	Peak Brake	0.16	0.99	2.1E+00	7.1E+01	1.0E+02
	Peak Accel	0.25	1.00	7.4E+00	4.7E+01	1.3E+02
	Peak Vertical	0.17	1.00	5.6E+01	7.0E+00	5.2E+01
	Peak Lateral	0.15	1.00	2.5E+01	3.3E+00	1.7E+01
	Peak Medial	0.17	1.00	7.0E+00	1.1E+01	3.0E+01
	Time Brake	0.19	1.00	9.9E+00	2.3E+01	7.2E+01
	Time Accel	0.06	1.00	1.9E+02	8.7E-01	1.2E+01
	Time Vertical	0.23	1.00	4.9E+00	1.1E+01	2.5E+01
	Time Lateral	0.22	1.00	2.2E+01	1.9E+00	9.0E+00
	Time Medial	0.18	1.00	8.1E+00	5.2E-01	1.5E+00
	Time BP	0.21	1.00	1.2E+01	1.4E+01	4.9E+01
	Cycle	0.15	1.00	3.5E+03	1.4E+00	3.9E+00

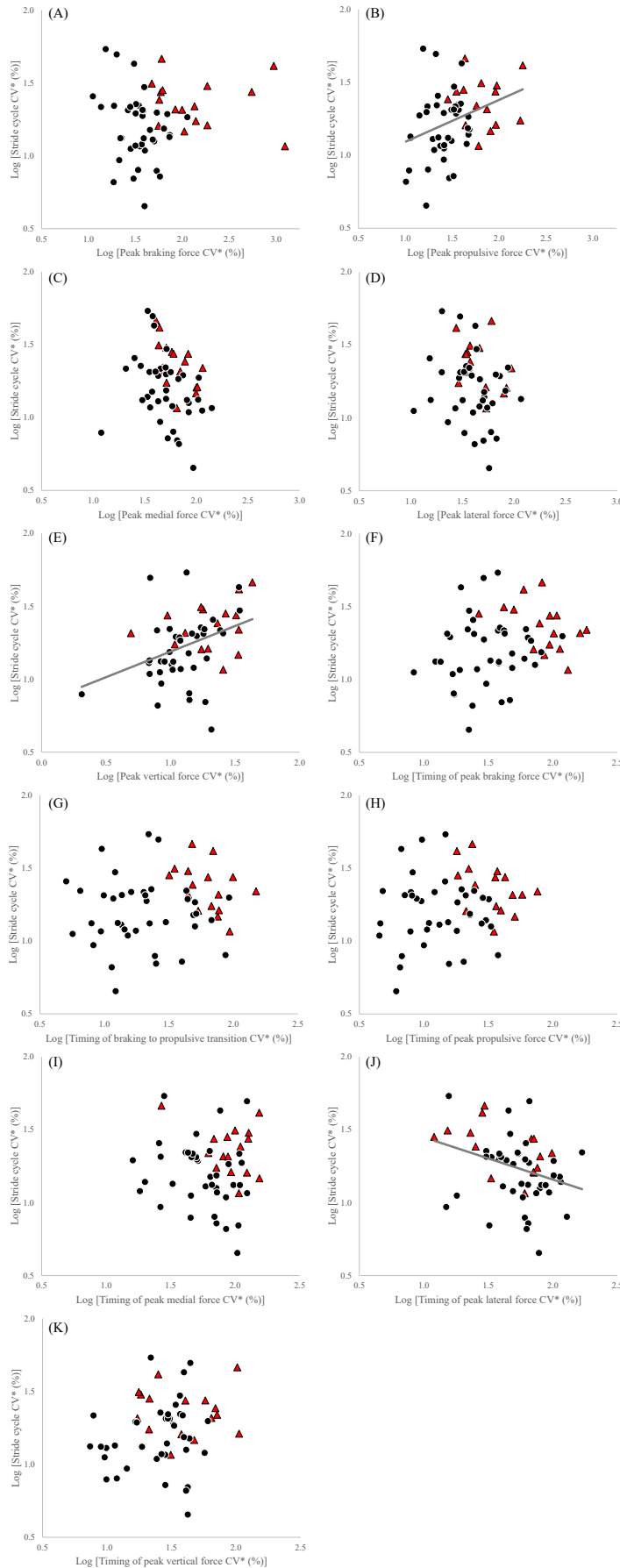
Supplementary Figures:



Supplemental Fig. 1. Scatterplots of the species-mean log-transformed coefficient of variation (CV^*) of (A) braking peak force, (B) propulsive peak force, (C) medial peak force, (D) lateral peak force, (E) vertical peak force, (F) timing of braking peak force, (G) timing of the braking to propulsive transition, (H) timing of propulsive peak force, (I) timing of medial peak force, (J) timing of lateral peak force, and (K) timing of vertical peak force as a function of species-mean log-transformed dimensionless speed CV^* (%). There is a significant negative relationship between species-mean log-transformed dimensionless speed CV^* (m/s) and peak braking force CV^* ($y = -0.53x + 2.41$; $P = 0.008$), the braking to propulsive transition CV^* ($y = -0.50x + 2.10$; $P = 0.007$) and the timing of peak medial force CV^* ($y = -0.31x + 2.22$; $P = 0.011$). Species with encapsulated Golgi tendon organs (GTO) are illustrated as black circles and species with unencapsulated GTOs are red triangles.



Supplemental Fig. 2. Scatterplots of the species-mean log-transformed coefficient of variation (CV^*) of (A) braking peak force, (B) propulsive peak force, (C) medial peak force, (D) lateral peak force, (E) vertical peak force, (F) timing of braking peak force, (G) timing of the braking to propulsive transition, (H) timing of propulsive peak force, (I) timing of medial peak force, (J) timing of lateral peak force, and (K) timing of vertical peak force as a function of species-mean log-transformed dimensionless speed. There is a significant negative relationship between species-mean log-transformed dimensionless speed (m/s) and peak braking force CV^* ($y = -0.32x + 1.59$; $P = 0.005$), peak medial force CV^* ($y = -0.13x + 1.69$; $P = 0.035$), the timing of peak braking force CV^* ($y = -0.33x + 1.50$; $P < 0.001$), the braking to , propulsive transition CV^* ($y = -0.39x + 1.30$; $P < 0.001$), the timing of peak propulsive force CV^* ($y = -0.33x + 1.10$; $P < 0.001$), the timing of peak medial force CV^* ($y = -0.15x + 1.76$; $P = 0.041$), and the timing of peak lateral force CV^* ($y = -0.26x + 1.62$; $P < 0.001$). Species with encapsulated Golgi tendon organs (GTO) are illustrated as black circles and species with unencapsulated GTOs are red triangles.



Supplemental Fig. 3. Scatterplots of the log-transformed species-mean coefficient of variation (CV^*) of stride cycle duration as a function of log-transformed CV^* of (A) braking peak force, (B) propulsive peak force, (C) medial peak force, (D) lateral peak force, (E) vertical peak force, (F) timing of braking peak force, (G) timing of the braking to propulsive transition, (H) timing of propulsive peak force, (I) timing of medial peak force, (J) timing of lateral peak force, and (K) timing of vertical peak force. There is a significant relationship between CV^* of stride cycle duration and peak propulsive force CV^* ($y = 0.29x + 0.81$; $P = 0.009$), peak vertical force CV^* ($y = 0.35x + 0.84$; $P = 0.005$) and the timing of peak lateral force CV^* ($y = -0.29x + 1.74$; $P = 0.016$). The solid line in each graph represents the best fit line. Species with encapsulated Golgi tendon organs (GTO) are illustrated as black circles and species with unencapsulated GTOs are red triangles.